PREPARATION OF Bi_2O_3 NANOSTRUCTURES AND THEIR LIGHT DRIVEN CATALYTIC ACTIVITY TOWARDS THE ERASURE OF TEXTILE DYES

CHRISTINA PREVITHA A/P JOHN DEVASAHAYAM

UNIVERSITI TUNKU ABDUL RAHMAN

PREPARATION OF Bi_2O_3 NANOSTRUCTURE AND THEIR LIGHT DRIVEN CATALYTIC ACTIVITY TOWARDS THE ERASURE OF TEXTILE DYES

CHRISTINA PREVITHA A/P JOHN DEVASAHAYAM

A project report submitted in partial fulfilment of
the requirements for the award of the degree of
Bachelor of Engineering (Hons) Environmental Engineering

Faculty of Engineering and Green Technology
Universiti Tunku Abdul Rahman

January 2016

DECLARATION

I hereby declare that this project report is based on my original work except for citations and quotations which have been duly acknowledged. I also declare that it has not been previously and concurrently submitted for any other degree or award at UTAR of other institutions.

Signature : _____

Name : Christina Previtha a/p John Devasahayam

ID No. : 11AGB01968

Date :

APPROVAL FOR SUBMISSION

I certify that this project report entitled **PREPARATION OF Bi_2O_3 NANOSTRUCTURES AND THEIR LIGHT DRIVEN CATALYTIC ACTIVITY TOWARDS THE ERASURE OF TEXTILE DYES** was prepared by **CHRISTINA PREVITHA A/P JOHN DEVASAHAYAM** and has met the required standards for submission in partial fulfilment of the requirements for the award of Bachelor (Hons) Environmental Engineering at Universiti Tunku Abdul Rahman.

Approved by,

Signature : _____

Supervisor : Dr. Lam Sze Mun

Date :

ACKNOWLEDGEMENT

This thesis would not have come to fruition without the help of various people in many ways. I would like to express my deepest and sincere appreciation to my supervisor, Dr. Lam Sze Mun for her constant guidance and patience. Without her encouragement, this thesis would not have been possible. Also, I would like to thank my co-supervisor, Dr. Sin Jin Chung for his support and guidance.

My sincere gratitude goes towards Universiti Tunku Abdul Rahman (UTAR), Kampar specifically the Faculty of Engineering and Green Technology in providing me a unique opportunity to undertake this research project. In addition, I would like to convey my most sincere gratitude towards the ever helpful laboratory officers who tirelessly try to cater to my every request in the laboratory. This goes out especially to Ms. Noor Hazreena binti Noor Izahar, Mr. Voon Kah Loon, Ms. Ng Suk Ting, Ms. Mirohsha a/p Mohan and lastly Mr. Chin Kah Seng.

Finally, my heartfelt appreciation goes towards my family members and coursemates for their unwavering physical and mental support throughout the duration of this project. I am especially grateful towards my coursemate and friend, Luk Mei Kwan, for her constant support and encouragement that have assisted me over the course of this project.

PREPARATION OF Bi_2O_3 NANOSTRUCTURES AND THEIR LIGHT DRIVEN CATALYTIC ACTIVITY TOWARDS THE ERASURE OF TEXTILE DYES

ABSTRACT

Azo dyes are widely used in the textile industry and as they exhibit undesirable aftereffect such as eutrophication, considerable amounts of research were dedicated towards its removal. Wide spectrums of technologies were devised and amongst them, heterogeneous photocatalysis incorporating bismuth trioxide (Bi_2O_3) surfaces as a potential means for wastewater treatment. Bi_2O_3 nanoflakes were synthesized via a co-precipitation method using cetyltrimethyl ammonium bromide (CTAB) as a surfactant. XRD, FESEM-EDX and UV-Vis DRS analyses were conducted to determine the crystal phase, morphology and band gap energy of the photocatalyst. The synthesised Bi_2O_3 was identified to be in the α-monoclinic phase and a determined band gap of 2.95 eV. The nanostructure was observed to be a flake-like Bi_2O_3 and had an average length of 250 nm and 60 nm thickness. The possible growth mechanism of Bi_2O_3 nanoflakes was also proposed. The photocatalytic activity of Bi_2O_3 nanoflakes were tested in the degradation of methyl green (MG) under fluorescent light irradiation. Comparison studies were conducted on commercial Bi_2O_3 and TiO_2 and were found that the Bi_2O_3 nanoflakes exhibited superior degradation of MG. Sedimentation test was conducted on the nanoflakes and commercial TiO_2 and was found that the nanoflakes settled well after 30 minutes as compared to TiO_2. The optimal operational parameters were determined to be 10 mM H_2O_2, 5 mg/L MG and pH 7. 100% of MG degradation was achieved within 20 minutes of irradiation while 81% of chemical oxygen demand (COD) was removed after 80 minutes of irradiation. Other dyes such as methylene blue (MB) and rhodamine B (RhB) could also be degraded by Bi_2O_3 under similar experimental conditions with their degradation efficiency in descending order MG > MB > RhB.

TABLE OF CONTENTS

LIST OF TABLES

LIST OF FIGURES

LIST OF SYMBOLS

•OH	Hydroxyl radicals
λ	Wavelength
A_0	Initial absorbance, abs
A_a	Absorbance at time *a*, abs
A_t	Absorbance at time *t*, abs
$BaSO_4$	Barium sulphate
$Bi(NO_3)_3 \cdot 5H_2O$	Bismuth nitrate pentahydrate
C	Concentration at specific time, mg/L
C_0	Initial concentration, mg/L
CO_2	Carbon dioxide
COD_0	Initial COD, mg/L
e^-	Electron
E_{bg}	Band gap energy
eV	Electronvolt
h^+	Hole
H^+	Hydrogen ion
H_2O	Water
H_2O_2	Hydrogen peroxide
HCl	Hydrochloric acid
HO^-	Hydroxyl ion
$HO_2^\bullet$	Perhydroxyl radical

hv	Photon energy
lx	Lux
mM	Millimole
NaOH	Sodium hydroxide
O_2	Oxygen
$O_2^{\bullet -}$	Superoxide radical
O_3	Ozone
W	Watt

LIST OF ABBREVIATIONS

2D	2-Dimensional
AOPs	Advanced Oxidation Processes
Bi_2O_3	Bismuth Trioxide
CB	Conduction Band
COD	Chemical Oxygen Demand
CTAB	Cetyl Trimethylammonium Bromide
FESEM-EDX	Field Emission Scanning Electron Microscope- Energy Dispersive X-Ray
MB	Methylene Blue
MG	Methyl Green
PTFE	Polytetrafluoroethylene
pzc	Point Zero Charge
RhB	Rhodamine B
SAOP	Semiconductor-Mediated Advanced Oxidation Process
Sc	Semiconductor
THM	Trihalomethane
TiO_2	Titanium Dioxide
USM	Universiti Sains Malaysia
UTAR	Universiti Tunku Abdul Rahman
UV	Ultraviolet
UV-Vis	Ultraviolet-Visible

UV-Vis DRS	Ultraviolet-Visible Diffuse Reflectance Spectroscopy
VB	Valence Band
XRD	X-Ray Diffraction

LIST OF APPENDICES

CHAPTER 1

INTRODUCTION

1.1 Wastewater in the dyestuff industry

The most widespread industrial use of dyes falls to the textile industry. As this is the largest industry, its average water consumption was 100 m^3/ton of product. In addition, it was estimated that there were more than 100,000 types of dyes available commercially with an annual production of up to 1,000,000 tons (Pang and Abdullah, 2013). The report added that the global demand for pigments and dyes were expected to grow at an average of 3.5% per year, from 1.9 million tons in 2008 to 2.3 million tons in 2013 and it is steadily increasing. It is because of this high demand in dyes that promoted the increase of dye presence in wastewaters. It is a widely recognized public perception that the water quality is greatly influenced by its colour. Colour is the first contaminant to be identified in wastewater (Crini, 2006).

Among the dyes, azo dyes are commonly used as colourants, consisting of one or more azo (-N=N-) bond couplings with several aromatic groups in their structure. (Rauf, Meetani and Hisaindee, 2011). They are the largest class (60-70%) of synthetic dyes used in the combination of textile, rubber, food, plastic, paper and cosmetic industry (Hosseini Koupaie, Alavi Moghaddam and Hashemi, 2011). These wastewaters are very stable in the environment and are resistant to oxidation and biodegradation. The dyes are a considerable source of aesthetic pollution, eutrophication and disruption of the aquatic ecosystem. Some azo dyes can be reduced to aromatic amines, which are potent carcinogens (Chen et al., 2015).

Furthermore, they are a well-known carcinogenic, mutagenic, allergic and cytotoxic agent that poses a threat to all life forms (Khandare and Govindwar, 2015).

Most of the dyes utilized in the textile industry are highly stable as they are intentionally designed to be able to resist biological, chemical and photolytic degradation. Other than the negative aesthetic effects of azo dyes, it is a hazardous material as a result of its slow biological degradation and their harmful intermediate degradation products (Papić et al., 2014). Hence, it is of utmost importance that these dyes require to be completely removed from the wastewaters.

According to Muhd Julkapli, Bagheri and Bee Abd Hamid (2014), the complete degradation of dyes were unable to be fully achieved through conventional methods such as adsorption, precipitation, flocculation, flotation, electrochemical, oxidation, reduction, biological, aerobic and anaerobic treatment as it was mentioned in various literatures that these methods have certain limitations such as production of secondary sludge production, lower efficiency, large area requirement and the costly affair of sludge disposal (Brillas and Martínez-Huitle, 2015; Hafshejani, Ogugbue and Morad, 2013; Saratale et al., 2010).

Weighing down these facts, much of the work at present focuses on the degradation and mineralization of synthetic dyestuff in the industry via heterogeneous photocatalyst (Muhd Julkapli, Bagheri and Bee Abd Hamid, 2014). Advanced oxidation processes (AOPs) have been gaining wide interest especially semiconductor mediated advanced oxidation process (SAOP). Heterogeneous semiconductor photocatalysis is an AOP and is considered as an outstanding method for the treatment of organic and inorganic pollutants in an aqueous suspension (Raza et al., 2016).

1.2 Problem statement

Wastewaters containing azo dyes are one of the most recalcitrant classes of organic compounds to treat. This is because according to Sreelatha et al. (2015), the presence of sulfo and azo groups in the dye structure protects the dye molecule from the attack of oxygenases, hence making them resistant to oxidative biodegradation. Dyes are highly dangerous as it could affect the photosynthesis activities within the aquatic system resulted from the decrease in light penetration. The presence of aromatics, metals and other materials within the dye makes them toxic towards certain marine life. Dyes are also carcinogenic, teratogenic or mutagenic in various species (Sreelatha et al., 2015). In addition, it can also cause severe damage to human beings such as dysfunctional reproductive system, kidneys, brain, liver and the central nervous system (Yagub et al., 2014). Therefore, it is crucial that the removal of dyes is properly dealt with. In this paper, three azo dyes will be focused on namely Methyl Green (MG), Methylene Blue (MB) and Rhodamine B (RhB).

Heterogeneous photocatalysis has proved to be of real interest as an efficient tool for degrading both aquatic and atmospheric organic pollutants. The heterogeneous photocatalysis involves the acceleration of photoreaction in the presence of a semiconductor photocatalyst (Gaya and Abdullah, 2008). Amongst the heterogeneous photocatalyst, titanium dioxide (TiO_2) proves to be the most destructive technology as reported by Konstantinou and Albanis in 2004. TiO_2 or titania is a very well-known and well-researched material as it has a stable chemical structure, physical, biocompatibility and electrical properties (Akpan and Hameed, 2009). TiO_2 is a conventional photocatalyst and is considered to be a semiconductor with a wide band gap (E_{bg} = 3.2 eV). Due to this high band gap, it can only be activated under UV irradiation with a wavelength of lower than 387 nm (Daghrir, Drogui and Robert, 2013).

In a report by Hameed et al. in 2009, bismuth trioxide (Bi_2O_3) has gained interest as it has an absorption edge at 2.8 eV with a suitable band edge potential for water oxidation, thermal stability and high refractive index. A *p*-type Bi_2O_3 heterogeneous semiconductor is considered as an efficient photocatalyst as it

possesses band gap energy in the visible region (Raza et al., 2016). It can oxidize water and produce highly reactive species for initiating oxidation reaction for the degradation of dyes, gases and drugs. Thus Bi_2O_3 was selected for this study to be utilized in the degradation of the three azo dyes.

1.3 Objective of study

Three dyes namely methylene blue (MB), methyl green (MG) and Rhodamine B (RhB) were selected as modal pollutants to be degraded by Bi_2O_3 under visible light. The objectives of this research are:

1. To synthesize nanostructure of Bi_2O_3 using a co-precipitation method
2. To characterize the synthesized Bi_2O_3 nanostructure using X-Ray Diffraction (XRD), Field Emission Scanning Electron Microscope-Energy Dispersive X-ray (FESEM-EDX) and Ultraviolet-Visible Diffuse Reflectance Spectroscopy (UV-Vis DRS) analyses
3. To determine the effect of parameters such as hydrogen peroxide concentration, initial dye concentration and solution pH on the photocatalytic degradation of dyes under fluorescent light irradiation

1.4 Scope of study

Bi_2O_3 nanostructure was fabricated through a co-precipitation method. The developed catalyst will be analyzed using XRD, FESEM-EDX and UV-Vis DRS analysis methods in order to characterize the morphology, size, structure, composition and band gap energy of the synthesized Bi_2O_3.

Three azo dyes namely MG, MB and RhB were selected as pollutants to be degraded. The photocatalytic test of these three dyes will be carried out using a batch photocatalytic reactor. The changes in dye concentration by Bi_2O_3 will be performed using a UV-vis spectrophotometer by measuring its absorbance. In addition, the mineralization extent of the photocatalyst will be measured using a COD analyzer.

CHAPTER 2

LITERATURE REVIEW

2.1 Azo dyes

Dye molecules were comprised of two significant components; the chromophores, responsible for the creating colour and the auxochromes, which can not only supplement the chromophore but also enhance the affinity of the dye molecules to attach towards the fibres and render it soluble in water (Gupta and Suhas, 2009). In another report, Clarke and Anliker (1980) mentioned that there were several ways of classifying commercial dyes whereby it can be catalogued in terms of its colour, structure and application methods.

Dyes could also be classified according to its solubility. Soluble dyes include direct, basic, acid, metal complex, reactive and mordant dyes. On the other hand, insoluble dyes encompass azoic, sulphur, disperse and vat dyes (Gupta and Suhas, 2009). Being a class, azo dyes are cost effective, exhibit good all round fastness properties and spans the whole shade range from yellow all through red and blue to green and strong (Waring and Hallas, 2013; Hunger, 2007). Azo dyes were defined by Singh, Singh and Singh (2015) to be electron deficient xenobiotic compounds as they possess electron withdrawing groups in the dye molecules that generated electron deficiency, making them resilient against degradation. These compounds attracted the electrons towards them and away from the main reaction required for the breakdown.

Azo dyes are chemically characterized by their nitrogen to nitrogen double bonds (-N=N). These are usually attached to two moieties in which typically were both aromatic groups; naphthalene rings or benzene, that can contain various substituents for instance methyl ($-CH_3$), chloro (-Cl), amino ($-NH_2$), nitro ($-NO_2$), carboxyl (-COOH), sulphonic ($-SO_3^-$) and hydroxyl (-OH), giving diversity to azo dyes (Saratale et al., 2011). Rauf, Meetani and Hisaindee (2011) added that depending on the number of (–N=N-) groups present in the molecule, azo dyes can be categorized into monoazo, diazo and triazo azo dyes and the cleavage of these bonds led towards the discolouration of dyes. Colour removal was connected to the number of azo bonds in the dye molecule. The colours of monoazo dyes were removed much faster comparative to the colour of the diazo and triazo dye (Erkurt, 2010).

The properties of azo dyes were enhanced to provide the dyes a high degree of biological and chemical stability, to resist breakdown due to sunlight exposure, time, soap and water. In other words, they were resilient towards degradation (Solís et al., 2012). As a huge amount of non-biodegradable dyes were released into receiving water bodies, it culminated towards a persistent, accumulative, mutagenic, carcinogenic and detrimental impact towards aquatic life, flora, fauna and the environmental matrix such as water and soil (Foo and Hameed, 2010).

Prolonged human exposure towards coloured effluents resulted in a wide spectrum of immune suppression, circulatory, respiratory, central nervous and neurobehavioral disorders indications such as vomiting, allergy, autoimmune diseases, salivation, cyanosis, leukaemia and lung edema amongst others (Verma, Dash and Bhunia, 2012).

Dye degradation, dye discolouration and dye removal are terms that are widely used in this field of research. Dye degradation was defined by Zhang et al. (2016) as the breaking down of the organic molecules into simpler forms such as CO_2, H_2O and other small molecules. In other words, any transformation of dyes resulted from irradiation and photocatalyst was considered as its degradation. For azo dyes, their degradation would mean its decomposition into simpler organic compounds by breaking of azo bonds and chromophores.

Discolouration of dyes was termed by Rai et al. (2014) as simply the disappearance of colour in the wastewater without any breaking of bonds. Discolouration does not necessarily coincide with the degradation of the dye molecules. They were determined by observing the absorbance reduction at the maximum wavelength of the dyes. Removal of dyes are quantified by determining the removal efficiency or percentage of dye removal using a formula.

In the present work, three azo dyes; MB, MG and RhB were utilized to undergo photocatalytic processes through heterogeneous photocatalytic reactions using Bi_2O_3. The structures and properties of these dyes are given in Table 2.1.

Table 2.1: Physical characteristics and molecular structure of Methylene Blue (MB), Methyl Green (MG) and Rhodamine B (RhB).

	Methylene Blue	**Methyl Green**	**Rhodamine B**
	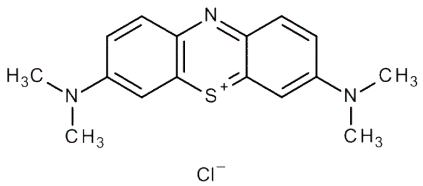	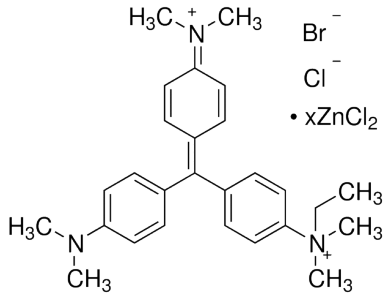	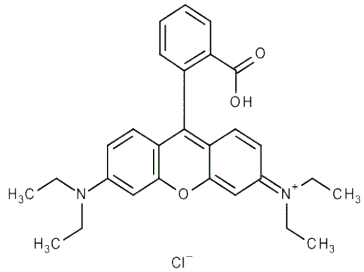
Alternate name	Basic Blue 9	Ethyl Green	Basic Violet 10
Abbreviation	MB	MG	RhB
Empirical formula	$C_{16}H_{18}ClN_3S$	$C_{27}H3_5BrClN_3 \cdot ZnCl_2$	$C_{28}H_{31}ClN_2O_3$
Molar mass	319.9 g/mol	653.24 g/mol	479.02 g/mol
C.I number	52015	42590	45170
Colour	Blue	Blue-Green	Red-light purple
λ_{max}	665 nm	631 nm	553 nm
References	Rauf, Meetani and Hisaindee, 2011; Wang et al., 2005	Geethakrishnan and Palanisamy, 2006	Al-Kadhemy, Alsharuee and Al-Zuky, 2011; Merouani et al., 2010

2.2 Methods of dye removal

Owing to the hazards of dyes in water bodies, inventions of a wide variety of treatment technologies has stimulated a dramatic progress in the scientific society. The available technologies for dye removal can be classified into three categories: physical, biological and chemical. These treatment methods were extensively used in handling the removal of dyes in order to ensure compliance with the environmental regulations which are increasing in stringency these days (Lam et al., 2012).

2.2.1 Physical treatment

Physical methods such as membrane-filtration processes, reverse osmosis, nanofiltration and electrodialysis were applicable for textile wastewater treatment (Abid, Zablouk and Abid-Alameer, 2012; Nataraj, Hosamani and Aminabhavi, 2009; Scialdone, D'Angelo and Galia, 2015). Electrodialysis is a process where the ionic components of the effluent were separated through semipermeable ion-selective membranes by an electrical potential (Tchobanoglous, Burton and Stensel, 2003). It was however mentioned by Ejder-Korucu et al. (2015) that the major disadvantage of the membrane technique was that they have a limited lifetime before membrane fouling begins to occur and the high cost of periodic replacements. To avoid membrane fouling in electrodialysis, it is vital that any suspended solids, colloids, turbidity and trace organics are to be removed prior to treatment (Ghaly et al., 2013).

Adsorption is also one of the leading methods applied to treat dyes from aqueous media. This treatment was categorized under physicochemical treatment method. There were large varieties of materials that were used as an adsorbent such as regenerated clay, rice bran and pine cone (Ogata, Imai and Kawasaki, 2015; Dawood and Sen, 2012; Meziti and Boukerroui, 2012). These authors reported having produced materials with effective adsorption capacities. However, this treatment came with a few restrictions such as the requirement of regeneration after material exhaustion and the loss of adsorption efficiency following regeneration (Salleh et al., 2011). In addition, adsorption presented the drawback of requiring

pretreatment of the wastewater to lower the suspended solid content before it was fed into the adsorption column and the eco-friendly disposal of the spent adsorbents (Paul, 2015; Mandal, 2014)

Physical or physicochemical treatments have several shortcomings whereby they are non-destructive in nature as they transfer the dye molecules to another phase rather than destroying them and are only effective when the effluent to be treated is small in volume (Vijayaraghavan, Basha and Jegan, 2013).

2.2.2 Biological treatment

Biological treatments for dyes usually involve aerobic and anaerobic processes (Malik and Grohmann, 2011). Microbial degradation of dyes were achieved through various microorganisms or instance yeast, bacteria, algae, fungi, phytoremediation and others (Tan et al., 2016; Tan et al., 2014; Daâssi et al., 2013; Tan et al., 2013; Zhou and Xiang, 2013; Doğar et al., 2010; Kagalkar et al., 2009; Saratale et al., 2009; Yang et al., 2009; You and Teng, 2009; Daneshvar et al., 2007; dos Santos, Cervantes and van Lier, 2007; Guo et al., 2007). The effectiveness of microbial discolouration heavily depends on the activity and adaptability of the selected microorganisms.

However, these treatments have its drawbacks in which biological treatments require large land area, has less flexibility in design and operation, are inhibited by sensitivity towards variation in toxicology of some chemicals and also takes a longer time for the discolouration-fermentation process (Yuan and Sun, 2010). Aerobic processes produces large amounts of biological sludge and required a huge disposal ground while anaerobic processes do not lower the pollutant content to a suitable level (Lam et al., 2012). Although many organic molecules were able to be degraded, many other recalcitrant materials were left behind due to the dye's complex chemical structure and synthetic organic origin (Crini, 2006). Particularly because of their xenobiotic nature, azo dyes are not totally degraded.

2.2.3 Chemical treatment

Processes such as oxidation, sodium hypochlorite (NaOCl) and chemical precipitation (coagulation) are some of the chemical treatment procedures that could be performed on wastewaters containing dyes. For one, the oxidation process has an advantage of application simplicity but on the flip side, this process requires the agent (H_2O_2) to be activated by some means (Salleh et al., 2011). The various methods of chemical oxidation vary depending on the way in which H_2O_2 is activated.

Other than direct oxidation, dyes can be removed electrochemically by indirect electrolysis whereby the main oxidizing agent was active chlorine, either in the form of gaseous chlorine (Cl_2), hypochlorous acid or hypochlorite ions, which were anodically produced from chlorides present or added into the solution (Panizza et al., 2007). Gogate and Bhosale (2013) reported that although the usage of chlorine gas was cost-effective, its use inevitably causes side reactions, producing organochlorine compounds including the toxic trihalomethane (THM). Generally, these chemical methods are costly and even though azo dyes were able to be effectively removed, the formation and accumulation of sludge caused a secondary disposal problem with an addition of excessive chemical usage leading towards the same problem (Sreethawong, 2012).

Although the treatment of azo dye-containing wastewater could be achieved with some of the available treatment processes, it was however only able to treat dye-containing wastewater to a certain extent as each process has its own degree of effectiveness. Granted that the physical, biological and chemical treatments have benefits, such processes produced large amounts of sludge and toxic by-products that have to be disposed of accordingly and also require substantial amounts of oxidant chemicals (Rahmani et al., 2015). In recent years, AOPs were considered as one of the most attractive methods of treating water containing toxic pollutants including organic dyes. Amongst the AOPs, heterogeneous photocatalysis offered to be a promising method and widely applied in the degradation of dyes.

2.3 Advanced oxidation process

AOPs were broadly defined by Klavarioti, Mantzavinos and Kassinos (2009) as aqueous phase oxidation techniques based on the production of highly reactive species such as primarily hydroxyl radicals (•OH) that led towards the destruction of target pollutants. This process, in which highly oxidizing species like •OH radicals are produced, can be created by the means of oxidizing agents such as H_2O_2, O_3, ultrasound, ultraviolet (UV) irradiation and catalyst (homogeneous or heterogeneous) (Atalay and Ersöz, 2015). Heterogeneous photocatalysis focuses on the use of semiconductors as a photocatalyst to aid in the degradation of dyes. As the process relies on the photoactivation of the semiconductor material, the efficiency of the catalyst is qualified by the semiconductor's capacity to generate electron-hole pairs with the addition of radical production (Muhd Julkapli, Bagheri and Bee Abd Hamid, 2014).

Cheng et al. (2016) stated the advantage of using AOPs above all biological and chemical processes was that they were extremely "environmental-friendly" as they neither produce massive amounts of hazardous sludge nor transfer pollutants from one phase to another as in adsorption and chemical precipitation. Other advantageous of AOPs are listed below (Abbas and Zaheer, 2014; Khataee and Kasiri, 2010; Poyatos et al., 2009):

1. Can be implemented under ambient conditions wherein atmospheric oxygen is adequate as an oxidant and may lead to the complete mineralization of organic carbon into CO_2.
2. Produce complete mineralization of wastewater dyestuff into CO_2, H_2O and inorganic compounds or into a more innocuous product.
3. Does not produce materials that require further treatment such as 'spent carbon' from activated carbon.
4. Rapid reaction rates.
5. Small footprint.

The main objective of AOPs is the generation of •OH in water. This radical is a powerful oxidant, is highly reactive and hence very short lived, and is non-selective electrophilic oxidizing agent (Naddeo, Rizzo and Belgiorno, 2011). The oxidation potentials of some important oxidizing agents are shown in Table 2.2 below. •OH is shown to possess the second highest oxidizing potential.

Table 2.2: Summary of Oxidants and Their Oxidation Potential (Naddeo, Rizzo and Belgiorno, 2011).

Oxidant	**Oxidation potential (eV)**
Fluorine (F_2)	3.03
Hydroxyl radical (•OH)	2.80
Atomic oxygen (O•)	2.42
Ozone (O_3)	2.07
Hydrogen peroxide (H_2O_2)	1.78
Perhydroxyl radical ($HO_2^{\bullet}$)	1.70
Hypochlorous acid (HOCl)	1.49
Chlorine dioxide (ClO_2)	1.36

2.3.1 Basic principles of heterogeneous photocatalysis

The photocatalytic process was termed as a photoinduced reaction in which was accelerated by the presence of a catalyst (Akpan and Hameed, 2009). Semiconductor molecules have a valence band (VB) which is occupied with stable energy electrons and an empty higher energy conduction band (CB). Photocatalytic reactions were initiated when a photoexcited electron was promoted from the filled VB of the semiconductor photocatalyst to the empty CB when the absorbed photon energy, *hv* was equal to or exceeds the band gap energy (E_{bg}) of the semiconductor photocatalyst ($hv > E_{bg}$), leaving behind a hole in the valence band (Gaya and Abdullah, 2008). From this, an electron-hole pair (e^--h^+) was generated. These charge carriers were then migrated to the surface of the catalyst where they were able to undergo redox reactions with organic pollutants (Daghrir, Drogui and Robert, 2013). The excited electron-hole pairs may either recombine without any chemical reactivity or migrate to the surface of the semiconductor and participate in the redox process whereby the electron proceeded to reduce the available chemical species while the hole engaged in the oxidation process (Adhikari et al., 2015).

The initiation of the photocatalytic reaction is through the irradiation absorption of a semiconductor (Sc), whereby it produces a hole (h^+) in the VB and electrons (e^-) in the CB. This is shown in Eq. (2.1) (Cheng et al., 2016).

$$Sc + hv\,(UV) \rightarrow Sc\,(e^-_{CB} + h^+_{VB}) \tag{2.1}$$

Once appropriate scavengers (H_2O and/or HO^-) are present, oxidation process takes place to form the reactive •OH radicals. This reaction is shown in Eqs. (2.2) and (2.3). Relevant reactions occurring on the surface of the semiconductor causing the degradation of dyes can be expressed by the following Eqs. (2.4) - (2.8) (Akpan and Hameed, 2009).

$$Sc(h^+_{VB)} + H_2O \rightarrow Sc + H^+ + \bullet OH \tag{2.2}$$

$$Sc(h^+_{VB)} + OH^- \rightarrow Sc + \bullet OH \tag{2.3}$$

$$Sc(e^-_{CB)} + O_2 \rightarrow Sc + O_2^{\bullet -} \tag{2.4}$$

$$O_2^{\bullet -} + H^+ \rightarrow HO_2^{\bullet} \tag{2.5}$$

$$\text{Dye} + \bullet OH \rightarrow \text{degradation products} \quad (2.6)$$

$$\text{Dye} + h^{+}_{VB} \rightarrow \text{oxidation products} \quad (2.7)$$

$$\text{Dye} + e^{-}_{CB} \rightarrow \text{reduction products} \quad (2.8)$$

In an aerated system, oxygen was reduced and in turn formed superoxides ($O_2^{\bullet-}$). This species later reacted with protons and adsorbed H_2O from the hydrated surface to produce perhydroxyl radicals ($HO_2^{\bullet}$) and hydrogen peroxide (H_2O_2), another source of •OH radicals (Lam, Sin and Mohamed, 2010). A schematic diagram illustrating the reaction taking place on the surface of TiO_2 is shown in Figure 2.1.

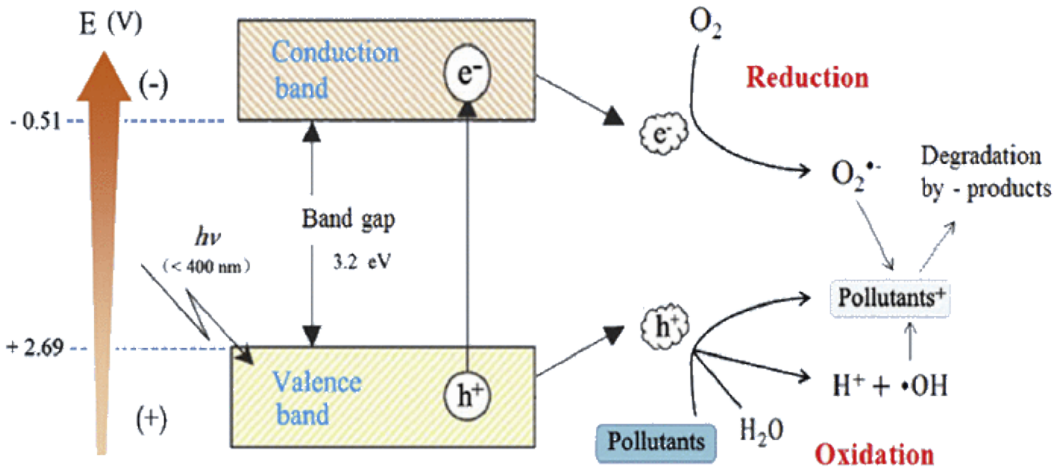

Figure 2.1: Schematic Diagram of the Reactions Taking Place on the Surface of a Semiconductor (Cheng et al., 2016)

2.3.2 Bi_2O_3 as semiconductors

Bi_2O_3 is a potential metal-oxide semiconductor with a direct band gap of 2.80 eV that is easily excited by visible light ($\lambda \geq 420$ nm) with a CB and VB edges at +0.33 and +3.13 eV respectively (Hameed et al., 2008). It is a common semiconductor extensively used in fields such as electronics and chemical engineering.

This semiconductor has three main crystallographic polymorphs symbolized by α-, β-, and γ- phases with an indirect band gap that differed for different crystal structures (Ho et al., 2013; Jalalah et al., 2015). The band gaps of α-, β-, and γ- Bi_2O_3 are 2.80eV, 2.58 eV and 2.80 eV respectively (Sun et al., 2012). The different phases of Bi_2O_3 are obtained by varying the temperature during the synthesis process. Amongst the various polymorphisms of Bi_2O_3, both α and β phases have been proven to be the most sensitive and effective photocatalysts to be operated under the visible light region (Cheng et al., 2010; Jalalah et al., 2015).

Salazar-Pérez et al., (2005) reported in their study that their selected starting materials, bismuth (III) nitrate and sodium borohydride, began oxidizing at 200°C using thermal oxidation. Phase transitions were observed at the temperature ranges of 200-750°C: β-Bi_2O_3 (200-300°C) to α-Bi_2O_3 (400-600°C) to γ-Bi_2O_3 (700-750°C). Figures 2.2a-c shows the crystal structures of α-, β-, and γ- Bi_2O_3 whereby the red and blue spheres indicate Bi and O atoms respectively.

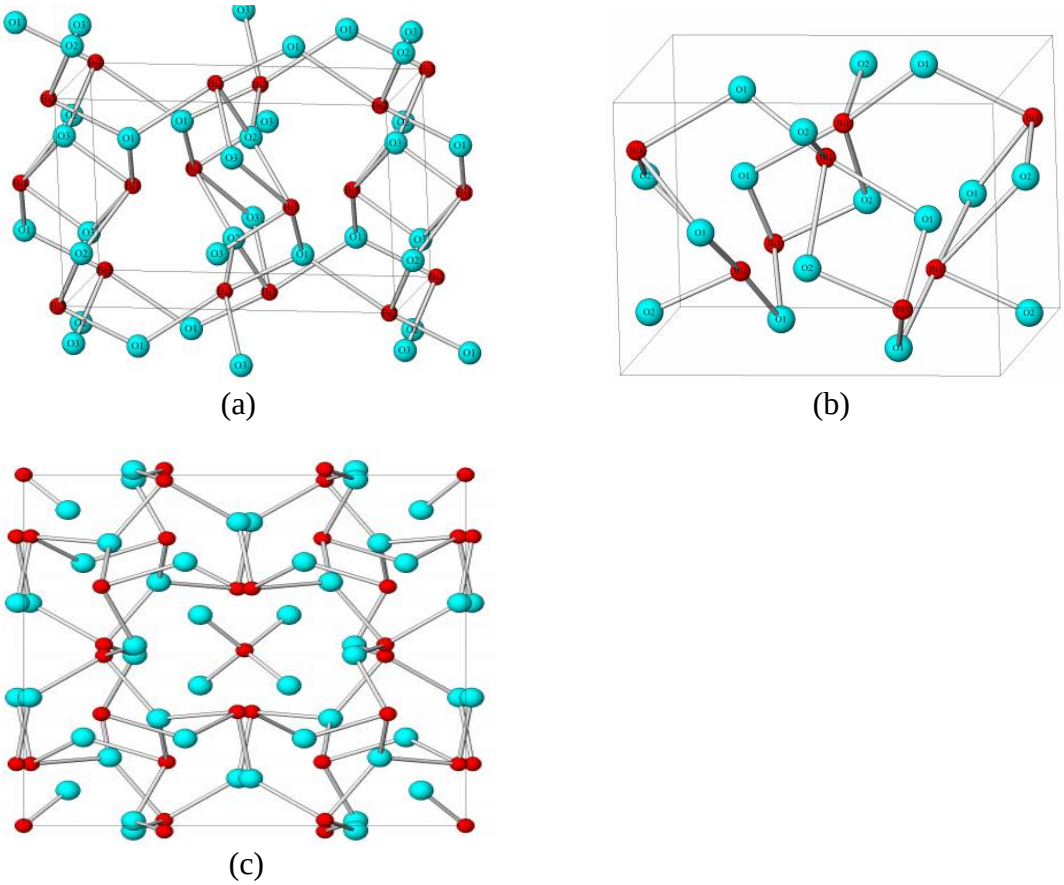

Figure 2.2: Illustrations of the Crystal Structures of (a) α-Bi_2O_3 (b) β-Bi_2O_3 and (c) γ-Bi_2O_3 (Thompson, 2010)

2.3.2.1 Synthesis of Bi_2O_3 nanostructures

Numerous techniques have been employed in the development of Bi_2O_3 nanostructures such as co-precipitation, hydrothermal, chemical precipitation, microwave-assisted, electrospinning, gel to crystalline conversion and others (Hou et al., 2013; Iyyapushpam, Nishanthi and Pathinettam Padiyan, 2013; Iyyapushpam, Nishanthi and Pathinettam Padiyan, 2012; Zhu et al., 2012; Huang et al., 2011; Wang, Zhao and Wang, 2011; Wang et al., 2009). Table 2.3 summarizes the relevant synthesis works of Bi_2O_3 nanostructures.

Table 2.3: Summary of relevant synthesis works of Bi_2O_3 nanostructures.

Synthesis route	Surfactants/ additives	Crystalline phase	Morphology	Reference
Chemical	Oleic acid	α-Monoclinic	Agglomerated crystals	Iyyapushpam et al. (2012)
Microwave-assisted	Ethylene glycol, Poly-ethylene glycol (PEG-400)	α- and β- Bi_2O_3	Crystalized sheet-like nanoparticles	Huang et al. (2011)
Electrospinning	Polyacrylonitrile (PAN)	β -Tetragonal	Nanofibers	Wang et al. (2009)
Sol-gel	Triton-X	α -Monoclinic	Compact rod-like/needle structure	Raza et al. (2015)
Hydrothermal	Benzyl alcohol	α- and β-Bi_2O_3	sheets(2D), nanowires, nanocrystals	Hou et al. (2013)
Co-precipitation	Poly-ethylene glycol (PEG-8000)	α -Monoclinic	Nanorods	Zhu et al. (2012)
Solvothermal	Ethylene glycol	β -Tetragonal	Nanospheres	Xiao et al. (2013)
Hydrothermal	L-Lysine	Phase selective α/β	Nanoflakes	Chen et al. (2011)
Sonochemical	-	α -Monoclinic	Nanorods	Sood et al. (2015)
Hydrothermal	-	α/γ composites	Agglomerated nanoparticles with smooth plate structures	Sun et al. (2012)

Chen at al. (2011) prepared a mesh-like Bi_2O_3 single crystalline nanoflake via bismuth oxalate as a precursor under different doses of lysine dispersant (as a crystal growth modifier) and different pH values and subsequently the effects of these variations in synthesis parameters on the morphology were studied. Their studies have shown that the different morphologies and crystalline phases have a significant impact on the photodegradation of RhB. Xiao et al. (2013) have accomplished in producing a 3-dimensional (3D) β-Bi_2O_3 nanospheres. From their report, the synthesized nanospheres exhibit an excellent removal percentage of acetaminophen (a human-derived pharmaceutical) at 93.6% compared to commercial Bi_2O_3 at 59.3% under visible light irradiation.

Oudghiri-Hassani et al. (2015) reported the synthesis of monolithic α-Bi_2O_3 nanoparticles via a solid-state reaction between the nitrate salt of bismuth and oxalic acid. The photodegradation of RhB was studied using this photocatalyst and it had shown a lower efficiency of photodegradation in which the degradation with the absence of photocatalyst took 16 min to be completed compared to the 12 min taken with the presence of photocatalyst under UV light irradiation. This could be inferred by the presence of $Bi_2(C_2O_4)_3 \cdot xH_2O$ and $Bi(C_2O_4)OH$ within the mixture signalling the existence of impurities. This concluded that various synthesis methods produced varying outcomes on the structure and consequently the photodegradation performance was affected.

In this current study, the co-precipitation method was selected as the synthesis route to produce Bi_2O_3. The advantages of using co-precipitation method include low costing, produces large quantities of particles with high purity and also being easy to use (Chu et al., 2013). Additionally, it enables control over the chemical composition of the synthesized product (Milenova et al., 2013).

Zhu et al. (2012) synthesized α-Bi_2O_3 and silver oxide (Ag_2O) nanoparticle composite photocatalysts. The Ag_2O-Bi_2O_3 composites were fabricated using the co-precipitation method. α-Bi_2O_3 nanorods were synthesized using bismuth nitrate pentahydrate and poly-ethylene glycol. The photocatalytic removal of MO was reported to be at 78% under visible light irradiation.

2.4 Parameter studies

Photocatalytic reactions are usually governed by many operating parameters such as photocatalyst loading, initial pollutant concentration, calcination temperature, light intensity, pH and temperature (Gaya and Abdullah, 2008). In this study, three parameters including initial dye concentration, solution pH and H_2O_2 concentration were discussed as to determine their role in the photocatalytic process of dye degradation.

2.4.1 Initial dye concentration

An increment in the initial dye concentration significantly reduces the degradation efficiency of the photocatalyst (Gnanaprakasam, Sivakumar and Thirumarimurugan, 2015). The explanation for this phenomenon was that an increase in dye concentration enabled more dye molecules to be adsorbed onto the surface of the photocatalyst causing most of the catalyst to be occupied (Gnanaprakasam, Sivakumar and Thirumarimurugan, 2015). These resulted in the unavailability of active sites to generate •OH thus reducing the photocatalytic activity (Schlesinger et al., 2013; Mai et al., 2008). Additionally, elevated dye concentrations decreased the path length or the number of photons that arrived on the surface of the photocatalyst, reducing the photoexcitation of electrons from the VB to CB. These resulted in decreased activity of the photocatalyst (Schlesinger et al., 2013; Sanatgar-Delshade, Habibi-Yangjeh and Khodadadi-Moghaddam, 2011).

This effect was proven in Sharma et al. (2011) report whereby the efficiency of photocatalytic activity increases with the increase in malachite green dye concentration. The activity of Bi_2O_3 then decreased upon concentrations of 2.00×10^{-5} M and above of the dye. Similarly, in Sharma et al. (2013) report, the efficiency of dye removal was observed to decrease with a further increase in dye concentrations above 1.8×10^{-5} M of Azure B. These two cases were attributed to the fact that after a certain concentration, the dye itself began to act as a filter for the incident light and do not permit the required light intensity to reach the surface of the

photocatalyst, decreasing the photocatalytic degradation of the dyes (Sharma et al., 2013).

2.4.2 Solution pH

It is crucial to study the role of solution pH on the removal of dyes (Gupta et al., 2012). The solution pH impacts the adsorption and dissociation of the dye molecules, oxidation potential of the VB, surface charge of the photocatalyst and also including the amount of charged radicals produced during the photocatalytic oxidation process (Gnanaprakasam, Sivakumar and Thirumarimurugan, 2015; Guo et al., 2014; Ananpattarachai, Kajitvichyanukul and Seraphin, 2009; Belessi et al., 2009; Li et al., 2008; Venkatachalam et al., 2007).

Barrera-Mota et al. (2015) in their research have found the optimal pH for the degradation of methyl orange (MO) dye using their synthesized β-Bi_2O_3 nanofilms to be at pH 3. This was associated with the surface charge of MO in an acidic nature as when tested in a neutral pH, the degradation activity was found to be very low. The observed discolouration at pH 3 was 80% in 180 min under UV light irradiation.

Sood et al. (2015) have synthesized α-Bi_2O_3 nanorods and have found that the point zero charge (pzc) of the nanorods were 4.6 and has exhibited a tremendous photocatalytic activity at a pH lower than 3 for the degradation of RhB. This is because in an acidic medium, it was discovered that perhydroxyl radicals ($HO_2^{\bullet}$) were formed. This radical in turn produced •OH. As a result, it caused the photocatalytic activity to increase. The observed degradation was 97% in 45 min under solar light irradiation.

2.4.3 H_2O_2 concentration

The e^--h^+ pair recombination that occurs in a photocatalyst can be reduced by the addition of some electron acceptors such as hydrogen peroxide (H_2O_2), ammonium persulfate ($(NH_4)_2S_2O_8$), potassium bromate ($KBrO_3$) and potassium persulfate ($K_2S_2O_8$) in order to increase the photocatalytic activity of the photocatalyst (Bazkiaei and Giahi, 2016; Gnanaprakasam, Sivakumar and Thirumarimurugan, 2015; Barka et al., 2013; Shanthi and Kuzhalosai, 2012). In most cases, H_2O_2 is more commonly used to increase the photocatalytic activity of the photocatalyst. Based on Eq. (2.9), H_2O_2 was able to generate •OH radicals through photolysis. In addition, H_2O_2 assisted in the trapping of e^- and hence prevented the recombination of e^--h^+ pair, producing more •OH radicals as a result as shown in Eq. (2.10). As a consequence, an improvement on the degradation of pollutants was able to be achieved. (Sapawe, Jalil and Triwahyono, 2013; Belgiorno and Rizzo, 2012; Tseng, Juang and Huang, 2012).

$$H_2O_2 + hv \rightarrow 2\ \bullet OH \tag{2.9}$$

$$H_2O_2 + e^- \rightarrow \bullet OH + OH^- \tag{2.10}$$

$$H_2O_2 + O_2^{\bullet -} \rightarrow \bullet OH + OH^- + O_2 \tag{2.11}$$

Conversely, beyond the optimum concentration of H_2O_2, an increased level of H_2O_2 decreased the degradation as observed in various literature reports due to the quenching effect of •OH radicals by H_2O_2 (de Lima et al., 2016; Dalbhanjan et al., 2015; Palácio et al., 2012; Saggioro et al., 2011).

Ma et al. (2014) demonstrated the effect of various H_2O_2 concentrations ranging from 2.5 mM of H_2O_2 to 15 mM H_2O_2 on the degradation of 2,4-dinitrophenol organic pollutant using ζ-Bi_2O_3/Bi_2MoO_6 composites. It was observed that using 5 mM of H_2O_2 resulted in a 100% removal of the dye within 40 minutes of a simulated solar light irradiation. An increase in concentrations above this optimum concentration exhibited an elongated degradation time of the pollutant with 15 mM H_2O_2 taking up to 80 minutes of irradiation before it was fully degraded.

Similarly, Samarghandi et al. (2015) reported the effect of various H_2O_2 concentrations on the photocatalytic degradation of pentachlorophenol (PCP) using ZrO_2 by varying the concentrations between 2.9 to 29.4 mM H_2O_2. The degradation

of PCP increased with an increase up to 14.7 mM H_2O_2, in which 100% of PCP was degraded in 30 minutes of UV light irradiation. An additional increase of H_2O_2 concentrations up to 29.4 mM resulted in a decrease in photocatalytic degradation whereby the degradation achieved was 77% in 30 minutes. It indicated the influence of the generated radicals on the degradation of PCP as at higher concentrations above 14.7 mM H_2O_2, •OH radicals were consumed by excess H_2O_2 to produce the less reactive perhydroxyl radicals ($HO_2^{\bullet}$). This in turn resulted in the lowered degradation efficiency.

2.5 Summary of literature review

Azo dyes are the largest group of dyes used in the textile industry. Effluents containing these dyes are difficult to be treated as they are engineered to be recalcitrant in nature. Conventional treatment processes such as physical, biological and chemical treatments on their own are only able to remove these dyes to a certain degree. Furthermore, some of these treatments produce additional problems such as sludge disposal and phase transfer of pollutants. Upon extensive research, AOPs have proved to be an attractive method in treating textile wastewaters. Hence, heterogeneous photocatalysis was selected in this study for the removal of azo dyes, namely MB, BG and RhB using Bi_2O_3. Bi_2O_3 as a photocatalyst possess a good potential in dye treatment as it can be activated under visible light irradiation. In this study, various Bi_2O_3 nanostructures will be synthesized using the co-precipitation method. Three operating parameters namely H_2O_2 concentration, initial pollutant concentration and solution pH will be studied in the degradation of dyes.

CHAPTER 3

RESEARCH METHODOLOGY

This chapter describes the experimental works for this report. The contents of the chapter are divided into eight subsections; materials and chemicals, apparatus, analytical procedure, preparation of photocatalyst, characterization of photocatalyst, photocatalytic activity, operational parameters and various dyes degradation studies. A flow chart of the overall work is given in Figure 3.1.

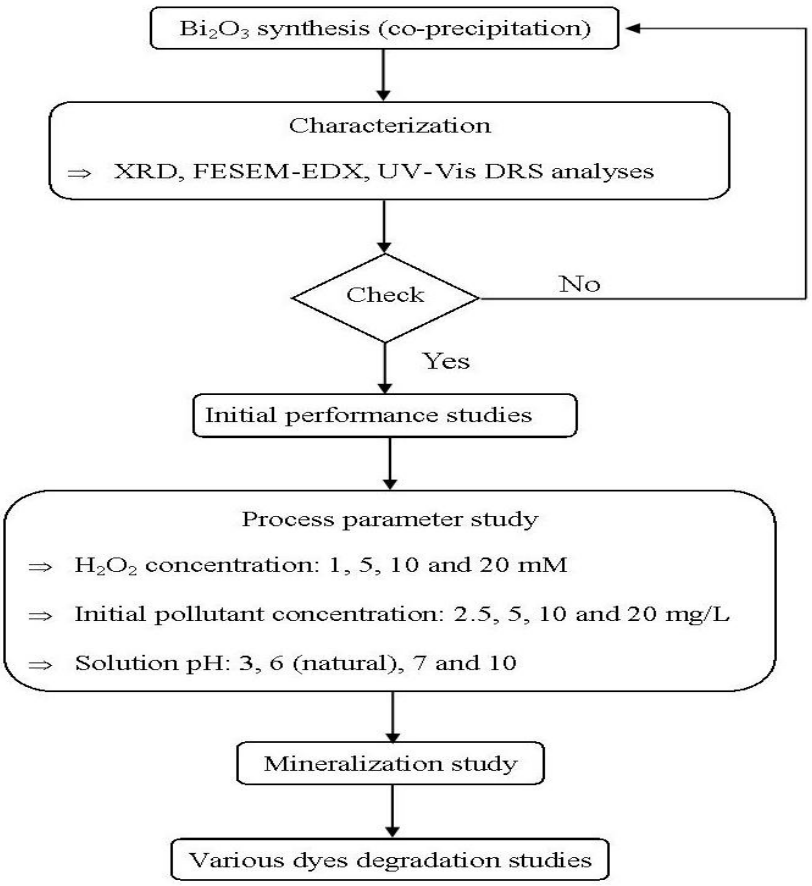

Figure 3.1: Flowchart of Experimental Work Involved in this Study.

3.1 Materials and chemicals

All the chemicals used were of analytical grade and used without further purification. Dye solutions were prepared by dissolving a certain amount of stock solution in distilled water (DI) (Favorit Water Still, 0.3 MΩ·cm). The chemicals used are listed in Table 3.1.

Table 3.1: List of Chemicals Used in this Study.

Chemical	Purity (%)	Supplier	Purpose
Bismuth (III) nitrate pentahydrate ($Bi(NO_3)_3 \cdot 5H_2O$)	98	Acros Organics	Photocatalyst preparation
Cetyl trimethylammonium bromide (CTAB)	99	Acros Organics	Photocatalyst preparation
Ethanol	95	HmbG Chemicals	Photocatalyst preparation
Commercial Bismuth (III) Oxide (Bi_2O_3)	99.9	Acros Organics	Photocatalyst comparison
Commercial Titanium Dioxide (TiO_2)	>98	Acros Organics	Photocatalyst comparison
MG	83	Aldrich	Model dye
MB	98.5	HmbG Chemicals	Model dye
RhB	90	Merck Millipore	Model dye
Hydrogen Peroxide (H_2O_2)	35	R&M Chemicals	Oxidizing agent
Hydrochloric Acid (HCl)	37	Quality Reagent Chemical (QreC)	pH adjuster
Sodium Hydroxide (NaOH)	50	Macron Fine Chemicals	pH adjuster
High Range COD Digestion Vials	-	HACH	COD analysis

3.2 Apparatus

The apparatus used and set-up of the experiment are shown in Figure 3.2. A schematic diagram of the set-up is shown in Figure 3.3. The photocatalytic reaction was performed in an acrylic black box as to prevent any leakage of UV light. The black box was equipped with two fans to provide ventilation and reduce heating within the box during the conduction of the experiments. In addition, air was bubbled from an air pump through a flow meter that was set to regulate the flow. The light source was provided by a 45 W compact fluorescent lamp (Universal) that held a 12 cm distance between itself and the surface of the model pollutant contained in a 250 mL beaker. A magnetic stirrer was used to provide constant stirring to keep the catalyst in constant suspension within the solution.

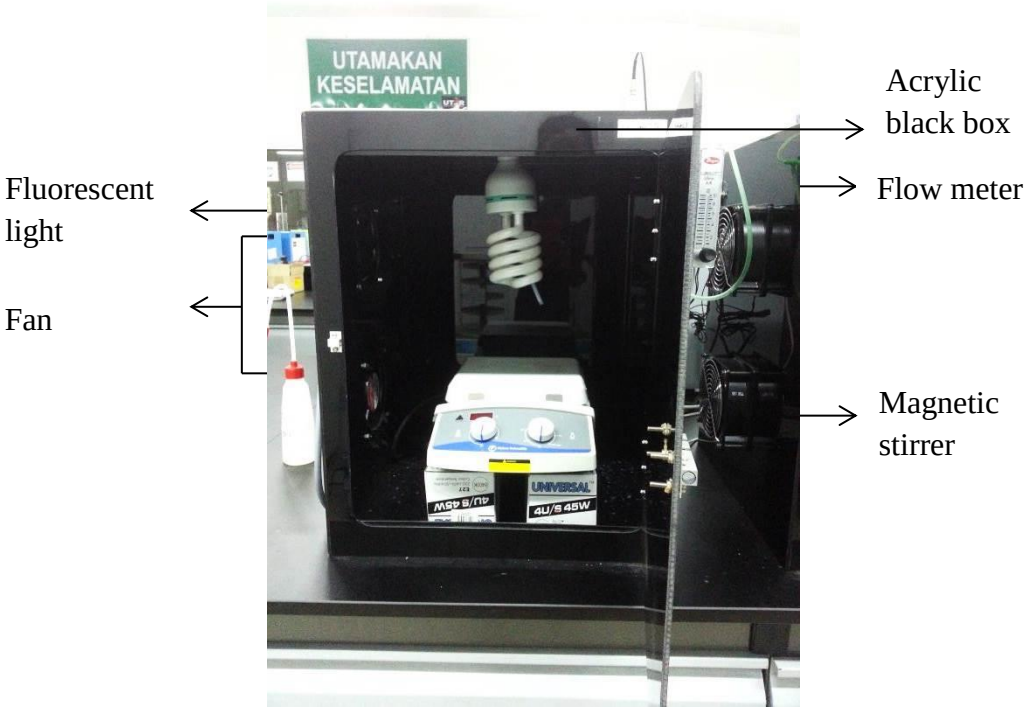

Figure 3.2: Experimental Set-up for Photocatalytic System.

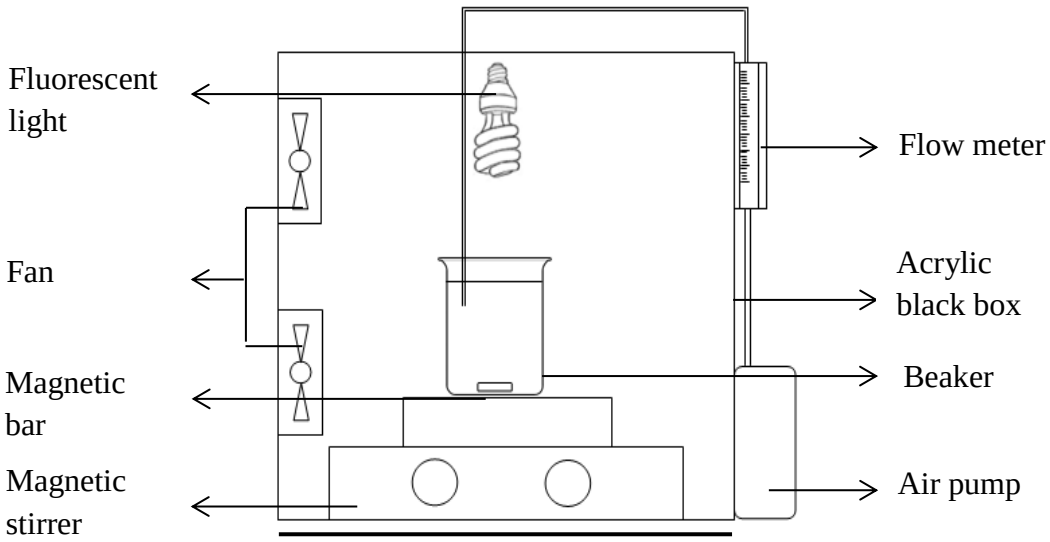

Figure 3.3: Schematic Illustration of Experimental Set-up.

3.3 Analytical procedure

3.3.1 UV-vis spectrophotometer analysis

A *Hach DR 6000* UV-vis spectrophotometer was used to monitor the concentration change of the dyes. The system uses a rectangular cuvette with a 1 cm internal size and the absorbance spectra for MG, MB and RhB were determined by measuring their respective maximum absorbance at a wavelength (λ) of 632, 664 and 553 nm respectively for each dye with distilled water as a blank sample (Merouani et al., 2010; Geethakrishnan and Palanisamy, 2006; Wang et al., 2005). All tests were performed in duplicate and the average values were used in the calculations. The absorbance of each dye was calculated using Eqn. (3.1).

$$\text{Absorbance (\%)} = \frac{A_0 - A_t}{A_0 - A_a} \times 100 \qquad (3.1)$$

where A_0 is the initial absorbance of the sample at a time equal to zero minutes (abs), A_t is the absorbance at time t minute (abs) and A_a is the absorbance at a time equal a minute (abs).

3.3.2 Chemical Oxygen Demand (COD)

To measure the mineralization extent during photocatalysis, the COD was measured using a *HACH DRB200* COD digital reactor. Prior to the COD measurement, 2 mL of sample was withdrawn and was tested for its COD measurement. The reactor block was preheated to 150°C prior to use and the samples were left in the reactor to react for 2 hours. Upon the completion of the reaction, the vials containing the samples were left to cool and were then measured using a *Hach DR 6000* UV-vis spectrophotometer. A blank was prepared using distilled water. The COD reduction was calculated using Eq. (3.2).

$$COD\ (\%) = \frac{COD_0 - COD}{COD_0} \times 100 \tag{3.2}$$

where COD_0 is the initial COD value at t=0 (mg/L) and COD is the COD value after a particular reaction time (mg/L).

3.4 Preparation of photocatalyst

Bi_2O_3 was synthesised via a co-precipitation method that was adapted from Hariharan et al. (2016). 100 mL (0.05 M) of bismuth nitrate solution was prepared using $Bi(NO_3)_3{\cdot}5H_2O$ and distilled water and was magnetically stirred and heated up. Subsequently, 1 g of cetyl trimethylammonium bromide (CTAB) was added into the solution. 5 M of NaOH was then added drop by drop until the colour of the mixture was observed to change from white to yellow under constant stirring at 80°C.

Upon cooling to room temperature, the as-formed yellow Bi_2O_3 precipitates were collected and followed by washing with ethanol and distilled water several times. After a drying treatment at 120°C for 3 h in an oven, the precipitates were calcined at 500°C for 2 h in a muffle furnace. Figure 3.4 depicts the schematic flow diagram for the synthesis process.

3.5 Characterization of photocatalyst

The as-synthesized Bi_2O_3 nanoflakes were characterized using standard XRD, FESEM-EDX, UV-Vis DRS analyses. XRD and FESEM-EDX analysis were performed in the Faculty of Engineering and Green Technology in University Tunku Abdul Rahman (UTAR), Kampar while UV-Vis DRS was performed at Universiti Sains Malaysia (USM), School of Chemical Science.

3.5.1 Crystal phase analysis

The crystal size and crystal phase of the fabricated Bi_2O_3 nanoflakes were characterized via X-ray Powder Diffraction (XRD) analyzer. The patterns were measured using a *Shimadzu X-ray Diffractometer (XRD-6000)* with a graphite monochromatic copper radiation (CuKα) with λ = 1.5418 Å. The scan rate was at 0.05° and 0.5 s^{-1} in the 2θ range of 20-60°.

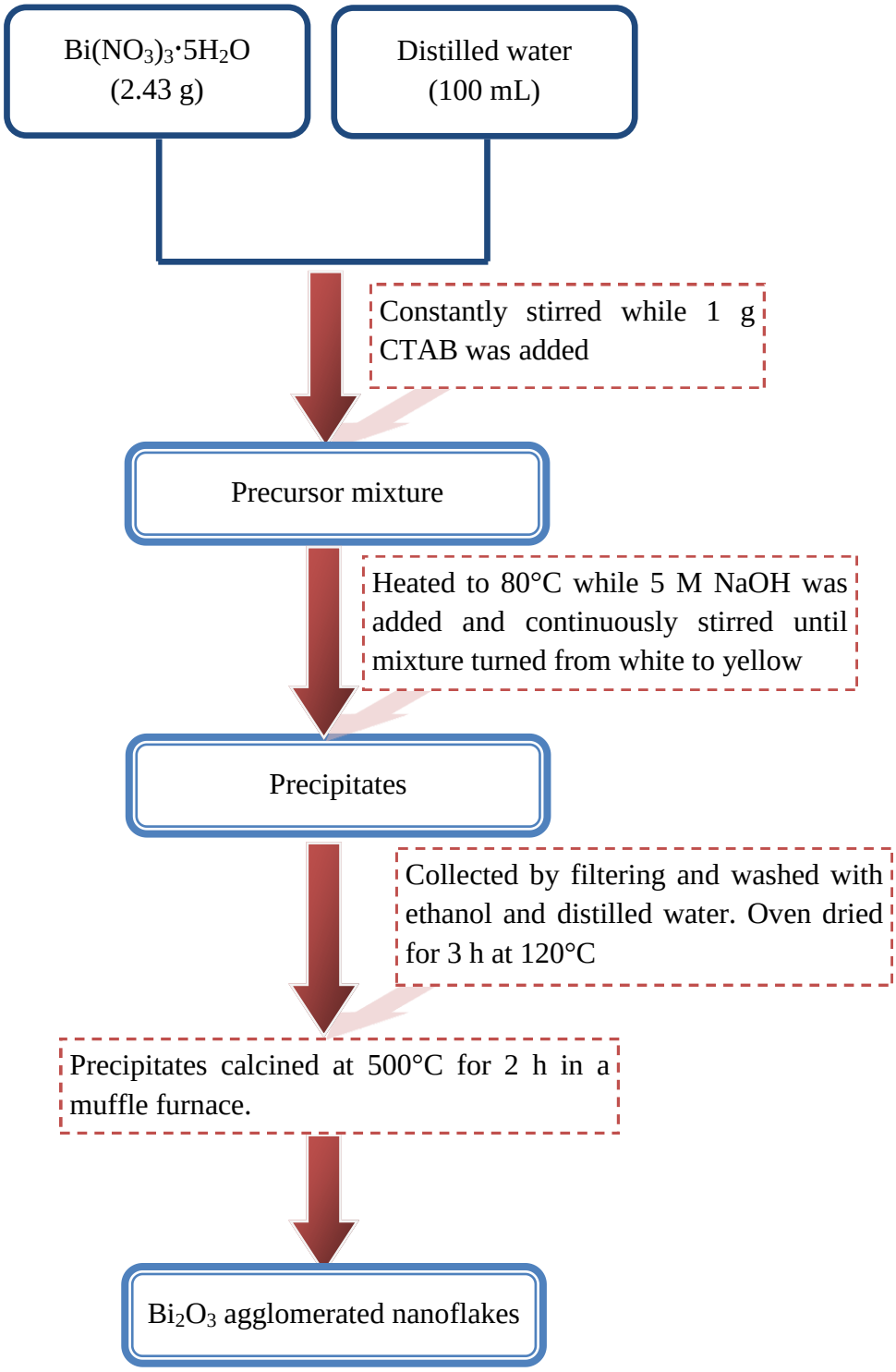

Figure 3.4: Schematic Flow Chart for the Synthesis of Bi_2O_3 nanoflakes.

3.5.2 Morphology analysis

A *Jeol JSM 7601-f* Field Emission Scanning Electron Microscope was used to measure the surface morphology of the as-synthesized Bi_2O_3 nanoflakes. FESEM analysis enables the measurement of the particle sizes of Bi_2O_3 nanoflakes. Prior to the analysis, carbon tape was used as a conductive adhesive for the Bi_2O_3 nanoflake samples on the aluminium stub.

Energy-dispersive X-ray Spectroscopy analysis was also carried out to determine the elemental composition of the as-synthesised Bi_2O_3 nanoflakes. EDX was conducted on the same analyser as FESEM and readings were taken from several spots on the Bi_2O_3 nanoflake samples.

3.5.3 Ultraviolet-Visible Diffuse Reflectance Spectroscopy (UV-Vis DRS) analysis

The band gap energy of the as-synthesized Bi_2O_3 nanoflakes was tested using an UV-Vis diffuse reflectance spectroscopy (DRS) *Perkin Elmer Lambda 35* UV-Vis spectrometer. The spectra were recorded in the range of 400 – 600 nm using $BaSO_4$ as a standard reference. The analysis was performed at Universiti Sains Malaysia (USM), School of Chemical Sciences.

$BaSO_4$ was placed in a quartz cell cuvette and held in the sample holder. Its spectrum was recorded. Upon completion, the cuvette containing the standard was removed and was replaced with Bi_2O_3 nanoflakes. The cuvette was placed back into the sample holder and was scanned for its corresponding absorbance spectrum from 400 – 600 nm.

3.6 Photocatalytic activity of Bi_2O_3 nanoflakes under UV-vis irradiation

Three dyes namely Methyl Green, Methylene Blue and Rhodamine B were used as model pollutants. The photocatalytic activities of Bi_2O_3 nanoflakes were evaluated under a compact fluorescent light. Experiments were conducted in a glass beaker of 250 mL whereby 100 mL of the dye to be degraded that contained 1 g/L of Bi_2O_3 nanoflakes were placed in a black box.

During all the experiments, air was bubbled through the solution via a tube at a fixed flow rate of 3 L/min. Constant mixing of the solution was also provided with an aid of a hotplate stirrer. Prior to the test, the solution was first kept in the dark for 30 minutes to ensure the adsorption-desorption equilibrium of the dye compound on the catalyst is reached. Later, the solution was irradiated under a 45 W compact fluorescent lamp (Universal) and the average light intensity reaching the reaction surface was 4100 lx. The light source was placed 12 cm above the reaction solution. During the reaction, 5 mL of the sample was collected at every 5 minutes and was centrifuged for 1 h to separate the Bi_2O_3 nanoflakes. Then, the supernatant was filtered using a PTFE membrane syringe filter (0.45 µm pore size) and subsequently analyzed using a UV-vis spectrophotometer and COD analyzer. The percentage of degradation was calculated using Eq. (3.3).

$$\text{Dye degradation (\%)} = \frac{C_0 - C}{C_0} \times 100 \tag{3.3}$$

where C_0 is the initial concentration of the dye at t=0 (mg/L), C is the concentration at a given time (mg/L).

3.7 Operating parameters studies

Photocatalytic reactions can be governed by many operating parameters such as photocatalyst loading, initial pollutant concentration, calcination temperature, light intensity, pH and temperature (Gaya and Abdullah, 2008). Three operating parameters namely H_2O_2 concentration, initial pollutant concentration and solution pH were selected in this work.

3.7.1 H_2O_2 concentration

To determine the effect of H_2O_2 as an oxidant on the photocatalytic activity of the dyes, various concentrations of H_2O_2 from 1 mM to 20 mM H_2O_2 was investigated. The concentration range was selected based on various literature reports (Petrović et al., 2015; Jakab et al., 2012; Abo-Farha, 2010). The experiment was conducted at a fixed condition using catalyst loading of 1 g/L with 5 mg/L MG concentration and at the natural pH 6.

3.7.2 Initial dye concentration

The effect of initial pollutant concentrations on the photocatalytic degradation was studied by varying the concentration of MG between 2.5 mg/L to 20 mg/L (Tayeb and Hussein, 2015; Martínez-de la Cruz and Obregón Alfaro, 2009). This experiment was conducted at a constant condition with catalyst loading 1 g/L at the natural pH of MG at pH 6.

3.7.3 Solution pH

The pH of the solution is an important parameter in the photocatalytic removal reactions on the surface of Bi_2O_3 nanoflakes as it dictates the surface charge properties of the photocatalyst (Barka et al., 2013). Hence, the photocatalytic degradation of the dyes were studied at different pH values including acidic (pH 3), neutral (pH 7), alkaline (pH 10) and natural pH of MG at pH 6. The solution pH was measured on a *HI 2550 HANNA Instruments* pH meter. The experiment was kept at a fixed condition at an initial dye concentration of 5 mg/L.

3.8 Various dyes degradation studies

Comparison studies between the degradation of various dyes were tested using different dyes namely MG, RhB and MB. The study was conducted to determine the feasibility of the as-synthesized Bi_2O_3 nanoflakes in the degradation of various dyes with different chemical structures. The experiment was conducted at photocatalyst loading = 1 g/L, H_2O_2 concentration = 10 mM, initial dye concentration = 5 mg/L and at pH 7.

CHAPTER 4

RESULTS AND DISCUSSION

This chapter presents the results and data analysis of the current research. The contents of the chapter were outlined into five subsections; characterization of photocatalyst, photocatalytic activity, process parameter, mineralization study and lastly comparative studies on various dyes.

4.1 Characterization of photocatalyst

Characterizations of the as-synthesized Bi_2O_3 nanoflakes were performed in order to assess its physicochemical and also optical properties. These properties were determined via XRD, FESEM, EDX and UV-Vis DRS. Determination of these properties enabled better understanding of the synthesized photocatalyst in terms of its efficient or inefficient performance in dye removal. XRD was utilized in the analysis of the crystal phase and the crystal structure of Bi_2O_3. The surface morphology and particle size of Bi_2O_3 was confirmed via FESEM while EDX revealed the elemental composition of the photocatalyst. The band gap energy (E_{bg}) was ascertained by means of UV-Vis DRS analysis.

4.1.1 Crystal phase analysis

Figure 4.1 depicts the XRD pattern of the synthesized Bi_2O_3 photocatalyst. Most of the prominent peaks in the range of 20°-60° were readily indexed to the monoclinic α-Bi_2O_3. It revealed that the prepared photocatalyst was in a single crystalline phase. The major peaks were observed at the angles of 2θ = 24.68°, 25.80°, 26.96°, 27.42°, 28.06°, 33.04°, 33.24°, 35.06°, 37.62°, 46.36°, 52.42° and 54.84° that corresponded to (- 1 0 2), (0 0 2), (1 1 1), (1 2 0), (0 1 2), (1 2 1), (2 0 0), (2 1 0), (1 1 2), (0 4 1), (- 3 2 1) and (- 2 4 1) crystal planes respectively. These results were also in accordance to other literatures that have obtained similar results from the JCPDS database (Hariharan et al., 2016; Karnan and Samuel, 2016; Jalalah et al., 2015; Karthikeyan, Udayabhaskar and Kishore, 2014). The sharp and strong diffraction peaks also implied that the photocatalyst possessed a good crystalline nature. In addition, Cheng et al. (2010) stated that the high crystallinity of α-Bi_2O_3 is favorable towards the decrease of recombination sites of the free carriers. This meant that more photogenerated e^--h^+ are able to partake in the photocatalytic activity and hence could result in a higher photocatalytic activity.

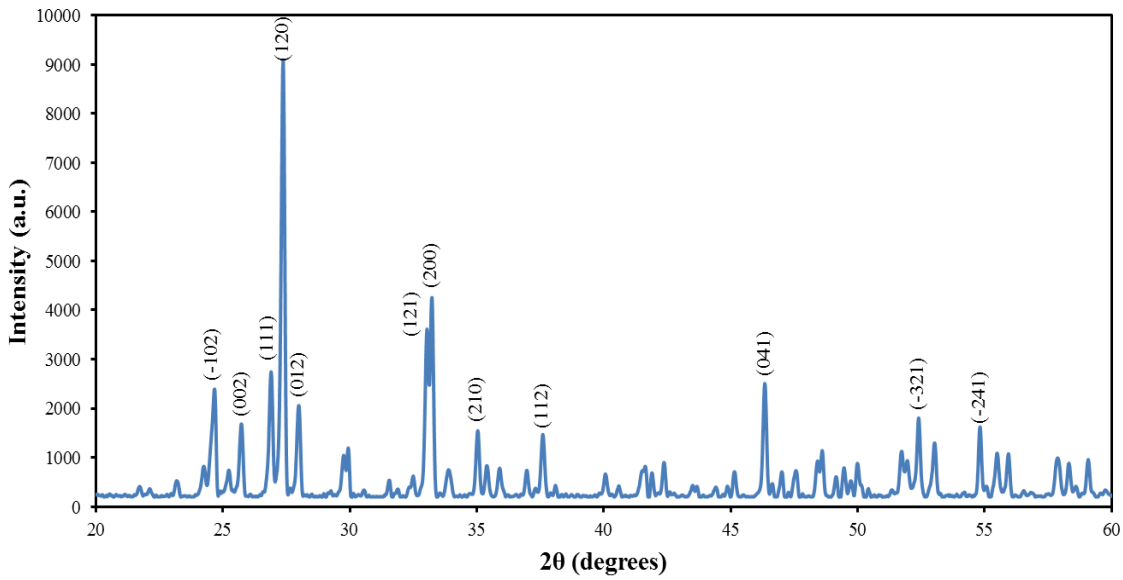

Figure 4.1: XRD pattern of synthesized Bi_2O_3 nanoflakes.

4.1.2 Surface morphology analysis

Figures 4.2a and b show the FESEM image of the as-synthesized Bi_2O_3 photocatalyst. It was identified that the morphology was of a 2D agglomerated nanoflake structure with an approximate average length of 250 nm and thickness of 60 nm. As seen from a lower magnification in Figure 4.2a, the as-synthesized Bi_2O_3 photocatalyst exhibited a cluster composed of flake-like rectangular shaped structures. Upon higher magnification (Figure 4.2b), it was revealed that the nanoflakes possessed smooth surfaces with a rounded edge. 2D nanostructures present a large percentage of active sites, enabling them to have highly reactive surfaces for photocatalytic reactions (Wang and Rogach, 2014).

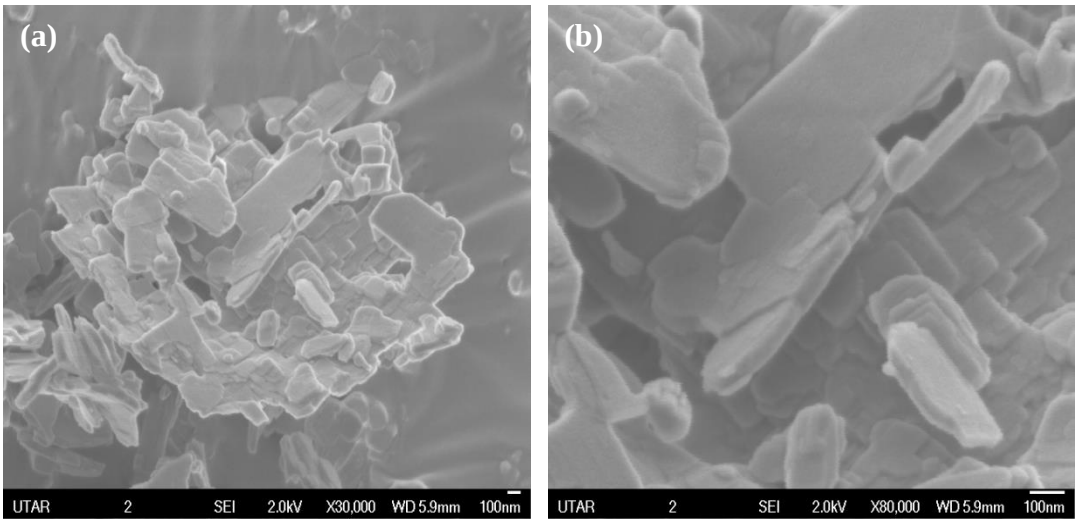

Figure 4.2: FESEM image of the as-synthesized Bi_2O_3 nanoflakes at a magnification of (a) × 30,000 and (b) × 80,000 magnifications.

In the current study, the growth mechanism of Bi_2O_3 nanoflakes was postulated based on the reaction processes in aqueous solution as follows (Eqs. (4.1) – (4.6)) (Mousa, Bayoumy and Khairy, 2013) :

$$Bi^{3+} + 3OH^- \leftrightarrow Bi(OH)_3 \quad (4.1)$$

$$Bi(OH)_3 \leftrightarrow Bi_2O_3 + H_2O \quad (4.2)$$

$$Bi(OH)_3 + OH^- \leftrightarrow [Bi(OH)_4]^- \quad (4.3)$$

$$CTAB \leftrightarrow CTA^+ + Br^- \quad (4.4)$$

$$[Bi(OH)_4]^- + CTA^+ \leftrightarrow CTA^+ - [Bi(OH)_4]^- \quad (4.5)$$

$$CTA^+ - [Bi(OH)_4]^- \leftrightarrow Bi_2O_3 + H_2O + CTA^+ \quad (4.6)$$

In a weakly basic solution, the starting material of $Bi(OH)_3$ dissolved to a smaller extent to form $[Bi(OH)_4]^-$ complex (Eq. (4.3)). The CTAB surfactant does not only accelerate the growth units' reaction, but it also led to their oriented growth (Mousa, Bayoumy and Khairy, 2013; Chen et al., 2012). CTAB is an ionic compound which is able to be completely ionized in water as shown in Eq. (4.4). $[Bi(OH)_4]^-$ existed in the form of a negatively charged tetrahedral while CTA^+ was positively charged with a tetrahedral head and a long hydrophobic tail. At the start of the CTAB-assisted solution process, $CTA^+ - [Bi(OH)_4]^-$ ion pairs were formed by an electrostatic interaction (Eq. (4.5)) between the dissociated CTA^+ and $[Bi(OH)_4]^-$. Later the $CTA^+ - [Bi(OH)_4]^-$ ion pairs formed the combination of CTAB and Bi_2O_3 as depicted in Eq. (4.6). These interactions lead towards the crystal growth of the $[Bi(OH)_4]^-$, resulting in the development of Bi_2O_3 nanoflakes.

4.1.3 EDX analysis

EDX measurements were conducted to identify the presence of Bi and O elements in the prepared nanoflakes. Figure 4.3 shows the EDX spectrum for the Bi_2O_3 nanoflakes. The spectrum showed the highest peak for Bi at 2.4 eV and for O at 0.6 eV approximately. The spectrum confirmed that the Bi_2O_3 nanoflakes were mainly composed of Bi and O based on atomic percent. It was determined that the elemental composition of the synthesized nanoflakes based on its atomic percent was 23.13% of Bi and 76.87% of O. The result also showed no other impurities were found in the as-synthesized nanoflakes.

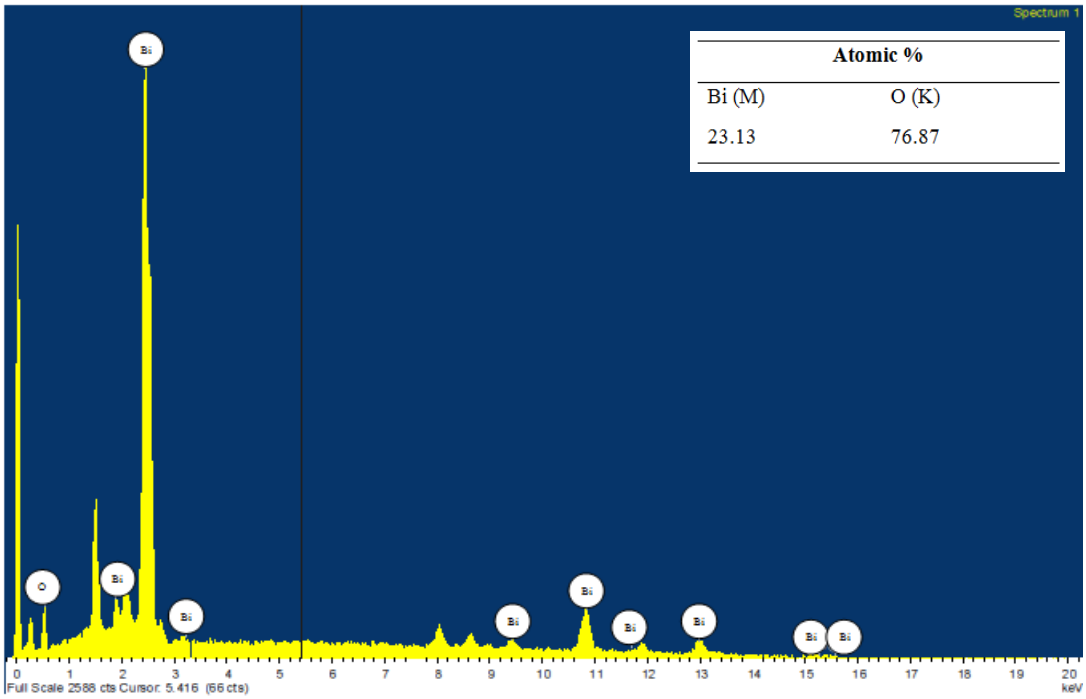

Figure 4.3: EDX spectrum and inset show the atomic percent of the synthesized Bi_2O_3 nanoflakes.

4.1.4 Ultraviolet-Visible Diffuse Reflectance Spectroscopy (UV-Vis DRS)

Figure 4.4 shows the UV-Vis DRS spectra of the as-synthesized Bi_2O_3 nanoflakes. The wavelength of the absorption edge was determined by extrapolation of the linear portion of the curve to the horizontal axis. The wavelength of the edge was defined by the intersection between them. The absorption edge was thus found to be approximately 420 nm. Subsequently, the band gap energy of the as-synthesized Bi_2O_3 nanoflakes were calculated using the Planck's equation (Eq. 4.3) (Benhebal et al., 2013).

$$E_{bg} = \frac{hc}{\lambda}$$

$$= \frac{1240}{\lambda} \qquad (4.3)$$

where E_{bg} is the band gap energy (eV), h is the Planck's constant (6.626×10^{-34} J·s), c is the speed of light (2.998×10^{8} m·s^{-1}) and λ is the wavelength (nm) of the absorption onset.

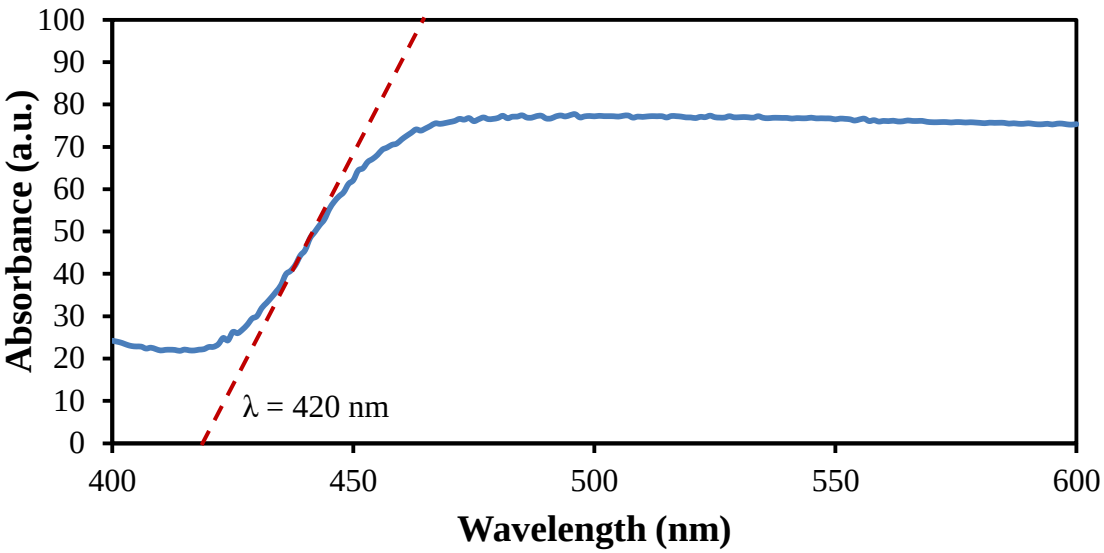

Figure 4.4: UV-Vis DRS spectra of synthesized Bi_2O_3 nanoflakes.

By applying the obtained wavelength into Eq. 4.3, the band gap was calculated to be 2.95 eV. This result was also supported by other literature reports (Hajra et al., 2015; Iljinas and Marcinauskas, 2015). It was worth noting that the absorption was more than 400 nm, indicating that the absorption edge was at the visible light region of the light spectrum. This was indicative that the synthesized Bi_2O_3 nanoflakes can be activated under visible light irradiation. Therefore, it was concluded that the Bi_2O_3 nanoflakes could be promising under sunlight irradiation.

4.2 Photocatalytic activities of the Bi_2O_3 nanoflakes

Figure 4.5 illustrates the UV-Vis absorption spectra of MG solution during different time intervals of the photocatalytic reaction conducted under fluorescent light irradiation. The absorption peak observed at 633 nm was due to the green color of the chromophore of MG (Bel Hadjltaief et al., 2015). Upon 20 minutes of irradiation, it was found that the peak corresponding to the chromophore almost disappeared. This confirmed the breaking of the azo bonds of the dye structure and hence its degradation (Sasikala et al., 2016; Cabansag et al., 2013).

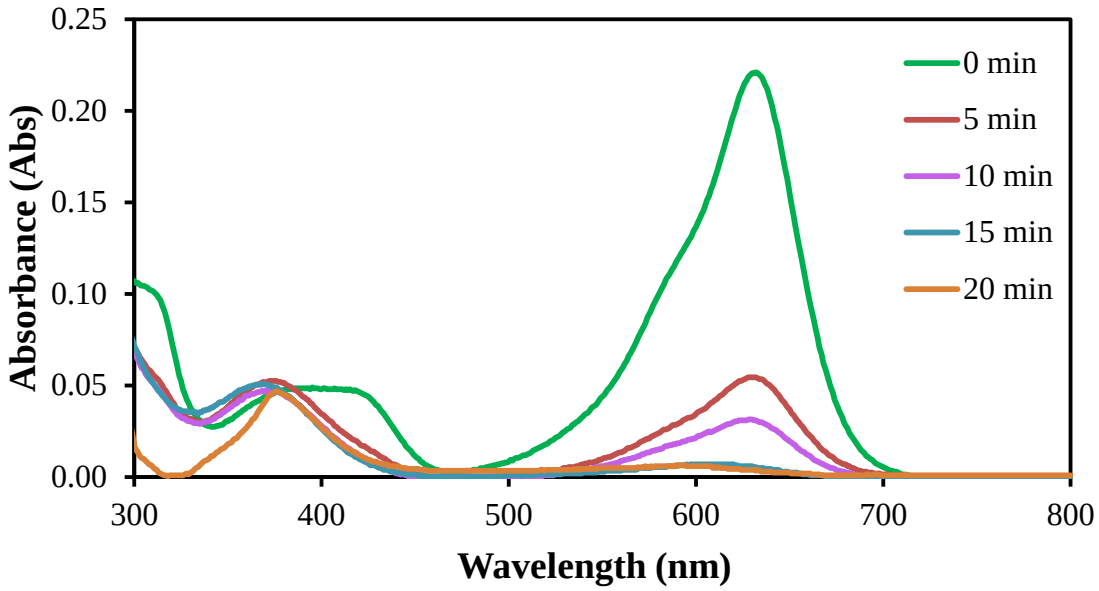

Figure 4.5: Evolution of UV-Vis spectra of MG solution with Bi_2O_3 nanoflakes at various time intervals ([MG] = 5 mg/L ; photocatalyst loading = 1 g/L ; [H_2O_2] = 10 mM ; natural pH of MG = 6).

The as-synthesized Bi_2O_3 nanoflakes were tested for its photocatalytic degradation of an azo dye, MG, under fluorescent light irradiation. In addition, H_2O_2 plays an important role in the photocatalytic activities of Bi_2O_3 nanoflakes. Its presence as an e^- accepting oxidizing agent was depicted to contribute towards improved photocatalytic activity by other researchers (Qiu et al., 2016; Deng et al., 2015; Felix, Andrew and Mededodec, 2014). Hence, its role was tested in the degradation of MG in the presence of Bi_2O_3 nanoflakes.

Figure 4.6 depicts the results of the conducted photocatalytic experiments on five various conditions on the removal of MG dye. As shown, the photolysis test resulted in 27% removal of MG within the irradiation time of 30 mins while during the dark run with the absence of fluorescent light irradiation, it was observed that the removal of MG was 63%. Two other tests were conducted in the presence of 10 mM H_2O_2 comparing the photocatalytic degradation of Bi_2O_3 nanoflakes with commercial Bi_2O_3 and commercial TiO_2. It was discovered that 100% degradation using Bi_2O_3 nanoflakes was obtained within 20 minutes while commercial Bi_2O_3 and TiO_2 exhibited a lower degradation with 79% and 68% respectively in 30 minutes of irradiation.

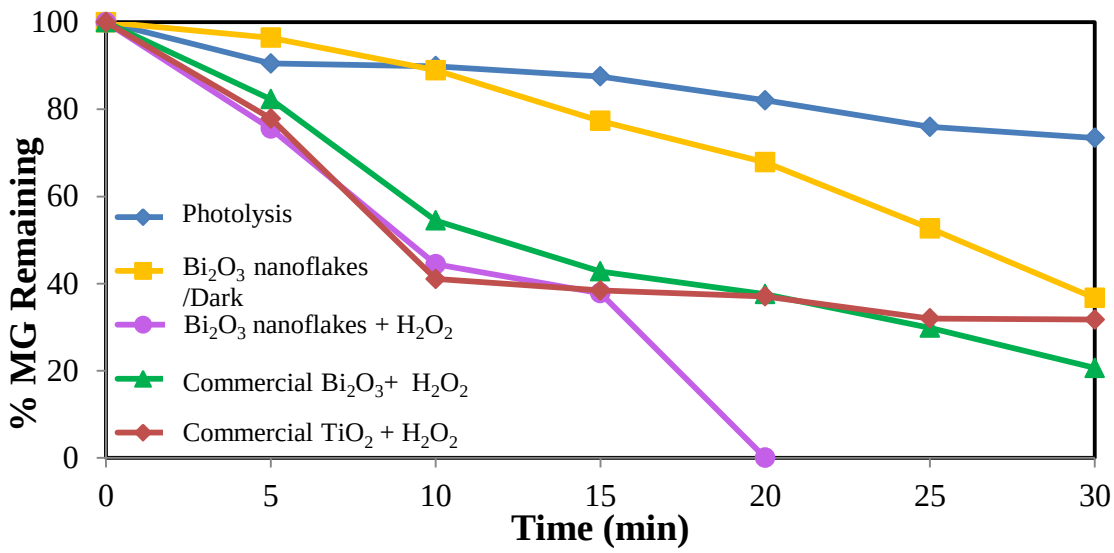

Figure 4.6: Photocatalytic experiments of MG degradation contained 10 mM H_2O_2 in photolysis, Bi_2O_3 nanoflakes, commercial Bi_2O_3 and commercial TiO_2 ([MG] = 5 mg/L ; photocatalyst loading = 1 g/L; natural pH of MG = 6).

Substantial degradation of MG was accomplished during photolysis. In a research carried out by Bousnoubra et al. (2016), it was stated that the elimination of the dye shows that MG possessed good absorbance of light thus leading to a decent removal during photolysis. The degradation of MG in the dark could be well attributed towards the direct adsorption of MG onto the surface of the Bi_2O_3 nanoflakes. This was supported by Chen et al. (2015) and Xu et al. (2015). Chen et

al. have succeeded in synthesizing various ratios of Bi_2WO_6/graphene oxide nanoflakes and had observed a maximum adsorption of 93.8% of RhB after 40 minutes in the dark while Xu et al. obtained approximately 25% removal of MB after 30 minutes dark adsorption using g-C_3N_4 nanoflakes. The large surface area of the as-synthesized photocatalyst provided more active sites for photocatalytic reactions.

The Bi_2O_3 nanoflakes exhibited excellent photocatalytic degradation of MG compared to both commercial Bi_2O_3 and TiO_2 in the presence of 10 mM H_2O_2. This could be well accredited towards the high crystallinity, morphology, surface area and band gap energy of the nanoflakes. Identical results were reported by Xiao et al. (2013) whereby their synthesized β-Bi_2O_3 nanospheres showed an outstanding 93.6% degradation of acetaminophen under visible light irradiation in 180 minutes. Commercial Bi_2O_3 and TiO_2 exhibited 59.3% and less than 10% degradation respectively. As high crystallinity corresponded with the towards the reduction of recombination sites of the photogenerated e^--h^+, the enhancement in the photocatalytic activity of Bi_2O_3 nanoflakes was possibly credited to its high crystallinity as compared to both commercial Bi_2O_3 and TiO_2 as there would be a presence of large amounts of reactive species production owing to the availability of e^--h^+ for the process.

In addition, the morphology and crystal size plays a vital role as well. As the synthesized Bi_2O_3 consisted of agglomerated nanoflakes, the offered number of active sites increased. 2D nanostructures have high surface areas and their small thickness contributed to a reduced distance for the photogenerated e^--h^+ to diffuse onto the surface (Cho et al., 2014). The crystal size of Bi_2O_3 nanoflakes was found to be approximately 250 nm in length while for commercial Bi_2O_3 and TiO_2 it was determined to be approximately 100 nm and 85 nm respectively (Hsieh et al., 2012; Ruslimie, Razali and Khairul, 2011; Martirosyan et al., 2009). The large particle size encouraged the photocatalytic degradation as it increased the number of active sites and light absorption to improve the generation of charge carriers (Park et al., 2015; Wang and Rogach, 2014).

Lastly, the band gap energy of the synthesized Bi_2O_3 nanoflakes was computed to be 2.95 eV, indicating that the photocatalyst had an extended light absorption of up to 420 nm (Magalhães et al., 2015). This meant that Bi_2O_3

nanoflakes were able to absorb a larger portion of the light spectrum up to the visible light region. Commercial Bi_2O_3 and TiO_2 had band gap energies of 2.80 eV and 3.15 eV respectively (Soroodan Miandoab and Fatemi, 2015; Anandan et al., 2010; Anandan and Wu, 2009). Both nanoflakes and commercial Bi_2O_3 were able to be effectively activated under fluorescent light. Due to its light absorption edge at 393 nm, TiO_2 can only be activated under UV light irradiation (Soroodan Miandoab and Fatemi, 2015). This meant that commercial TiO_2 was inefficient under fluorescent light irradiation. Fluorescent light was used as an imitation source for natural sunlight irradiation. The photon energy emitted from the irradiation source was not strong enough to separate the e^--h^+ pair (Hay et al., 2015). As a result, the photocatalytic activity of TiO_2 was observed to be reduced as only a small portion of UV light was available to be absorbed.

An economical photocatalyst should provide an ease of particle separation and their recovery from the reaction system upon completion of the photocatalytic activity (Pamt et al., 2013). A sedimentation test was carried out to compare the performance of Bi_2O_3 and commercial TiO_2. The samples after its photocatalytic activity were left untouched for 30 minutes. Figure 4.7a and b show the sedimentation performance of Bi_2O_3 and commercial TiO_2 respectively. It was observed that after 30 minutes, the samples containing Bi_2O_3 to be less turbid with a visible layer of photocatalyst at the bottom of the beaker while commercial TiO_2 exhibited a more turbid mixture with no visible layer of settled photocatalyst. This could be attributed to the density of the photocatalyst. The densities for Bi_2O_3 and TiO_2 are 8.9 g/cm^3 and 4.23 g/cm^3 respectively (Perry, 2016; Zhang et al., 2012). The higher density of Bi_2O_3 promoted the sedimentation of the photocatalyst. This factor could boost the ease of recovery of the photocatalyst from the aqueous suspension for its reusability when applied in wastewater treatments.

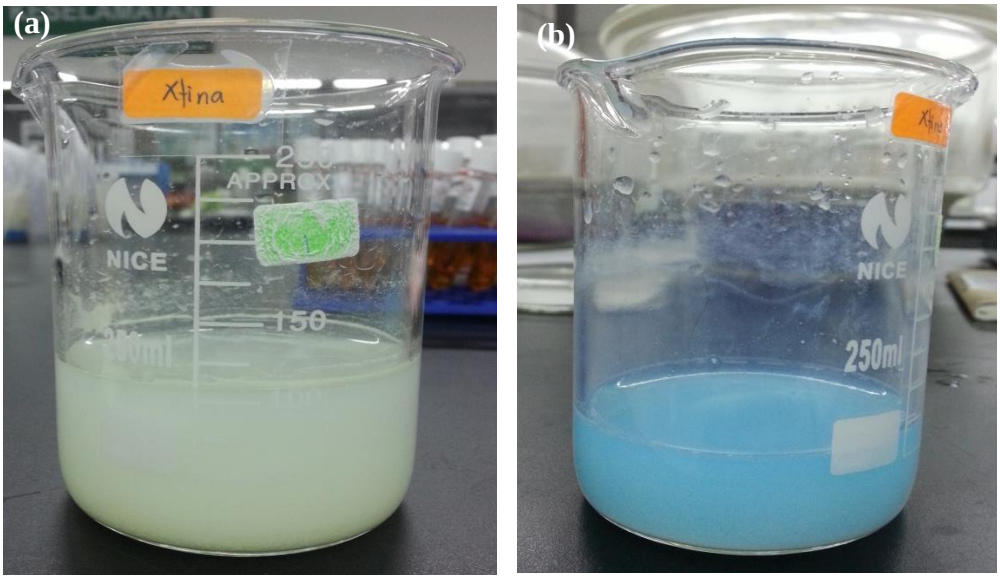

Figure 4.7: Sedimentation test after 30 minutes of MG photocatalytic activity using (a) Bi_2O_3 nanoflakes and (b) TiO_2 photocatalysts.

4.3 Process parameter studies

4.3.1 Effect of H_2O_2 concentration

Figure 4.8 illustrates the effect of various H_2O_2 concentrations on the photocatalytic degradation of MG. It was observed that in the absence of H_2O_2, the degradation of MG within 20 minutes of fluorescent light irradiation was 26.9%. However, the addition of H_2O_2 showed a significant effect on the degradation of MG. A decrease in degradation was seen with an increase in H_2O_2 concentration from 1 mM to 5 mM H_2O_2 from 50.1% to 32.1%. Complete degradation was attained at 10 mM of H_2O_2 within 20 minutes. This degradation efficiency then decreases with an increase of H_2O_2 concentration up to 20 mM (43.5%). Therefore, the best H_2O_2 concentration was found to be 10 mM H_2O_2.

.

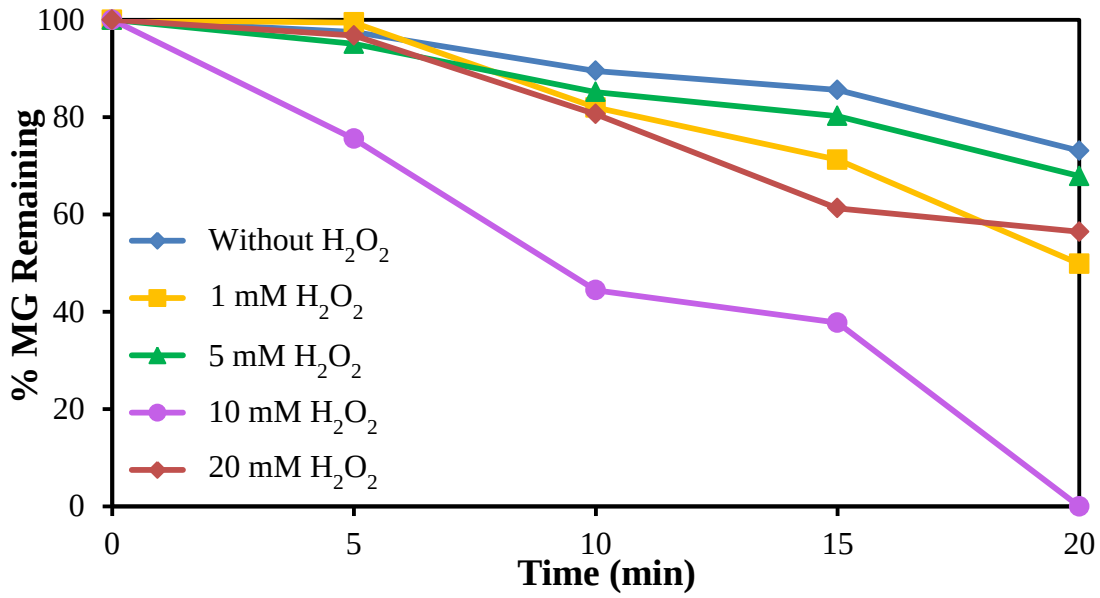

Figure 4.8: Effect of various H_2O_2 concentrations on the photocatalytic degradation of MG ([MG] = 5 mg/L ; photocatalyst loading = 1 g/L ; natural pH of MG = 6).

Several researchers have studied the effect of H_2O_2 concentrations on the degradation of various organic pollutants using Bi_2O_3. Yin et al. (2010) studied the effect of H_2O_2 on the degradation of pentachlorophenol (PCB) using Ti-doped β-Bi_2O_3. They found that 30.1% of PCB was degraded using 10 mM H_2O_2 under 30 minutes of visible light irradiation. In another report, Ma et al. (2014) tested the effects of H_2O_2 concentrations ranging from 2.5 to 15 mM for the degradation of 2,4-dinitrophenol via ζ-Bi_2O_3/Bi_2MoO_6 composites. They discovered that at 15 mM H_2O_2, 90% of 2,4-dinitrophenol was degraded within 80 minutes of visible light irradiation.

The enhancement of the rate of photocatalytic activity was mainly attributed towards two reasons. First was that H_2O_2 was a better electron acceptor than molecular oxygen as they have an oxidation potential of 1.78 eV and 1.23 eV (Giménez and Bisquert, 2016; Viswanathan, Hansen and Nørskov, 2015). Secondly, H_2O_2 may photolytically split directly to produce •OH radicals under UV light irradiation (Li et al., 2011). H_2O_2 increased the production of •OH radicals through the reduction of H_2O_2 at the CB as shown in Eq. (4.4) or even if H_2O_2 was not

reduced at the CB, it would accept an e^- from the superoxide ($O_2^{\bullet-}$), producing •OH radicals (Eq. (4.5)) (Sapawe, Jalil and Triwahyono, 2013).

$$H_2O_2 + e^- \rightarrow \bullet OH + OH^- \quad (4.4)$$

$$H_2O_2 + O_2 \rightarrow \bullet OH + H^+ + O_2^- \quad (4.5)$$

At higher concentrations above 10 mM, the H_2O_2 adsorbed onto the surface of the photocatalyst could very effectively scavenge the •OH radicals formed and inhibit the major pathway for the heterogeneous generation of •OH radicals. The reactions are shown in Eqs. (4.6) and (4.7) (Tseng, Juang and Huang, 2012; Modirshahla, Behnajady and Jangi Oskui, 2009). The formed $HO_2^\bullet$ as a result of excess H_2O_2 were known to be less reactive than •OH radicals (2.80 eV) with an oxidation potential of 1.70 eV and as a consequence, the degradation decreased as a longer period of time was required to achieve complete degradation.

$$H_2O_2 + \bullet OH \rightarrow HO_2^\bullet + H_2O \quad (4.6)$$

$$HO_2^\bullet + \bullet OH \rightarrow H_2O + O_2 \quad (4.7)$$

4.3.2 Effect of initial dye concentration

The effects of initial MG concentrations were studied in the concentration range of 2.5 to 20 mg/L. As shown in Figure 4.9 the degradation efficiency of MG increased from 2.5 mg/L to 5 mg/L up to 100% for 5 mg/L in 20 minutes under fluorescent light irradiation and subsequently decreased upon this point to 24.2% for 20 mg/L. This demonstrated the best MG concentration was found at 5 mg/L.

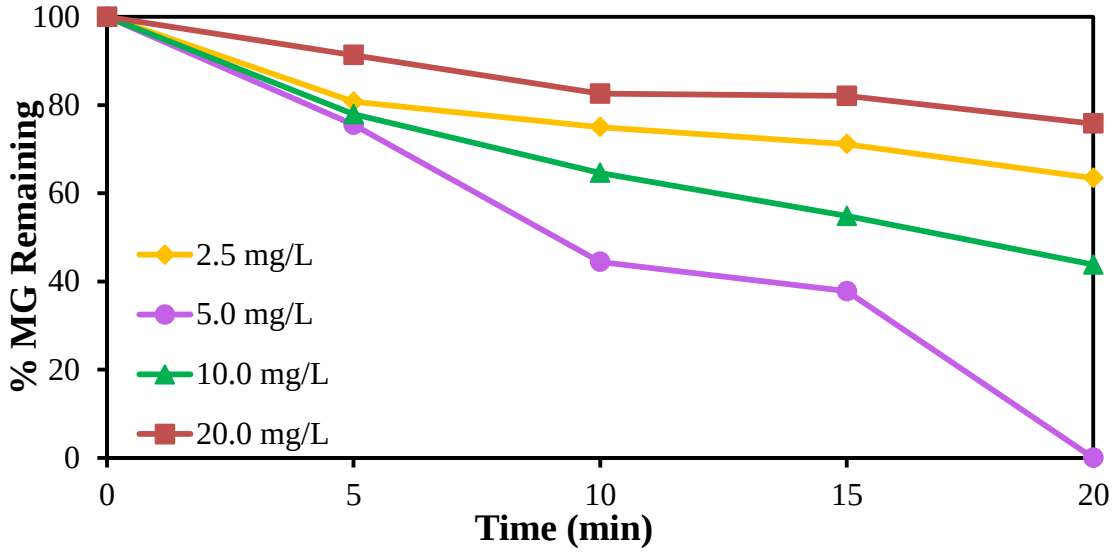

Figure 4.9: Effect of various initial dye concentrations on the degradation of MG in the presence of 10 mM H_2O_2 (photocatalyst loading = 1 g/L ; natural pH of MG = 6).

The increase in photocatalytic degradation of dyes with an increase in initial dye concentration up to an optimum concentration have been documented by several literature reports (Ambreen et al., 2014; Mohaghegh et al., 2014; Ameta, Ameta and Ahuja, 2013; Kumawat, Bhati and Ameta, 2012; Avasarala, Tirukkovalluri and Bojja, 2010). Ambreen et al. (2014) tested the effect of various initial concentrations of RhB on its degradation by varying them from 2.5 – 17.5 mg/L using Ta_2O_5 photocatalyst under UV irradiation. The photocatalytic degradation increased up to 12.5 mg/L and subsequently decreased at 17.5 mg/L. 90% of degradation was obtained within 150 minutes using 12.5 mg/L where else 70% of RhB degradation was achieved for 2.5 mg/L under the same irradiation time. Avasarala, Tirukkovalluri and Bojja (2010) experimented on the degradation of various concentrations of monocrotophos (MCP), an organophosphate insecticide, using Be-doped TiO_2. They tested on a concentration range of 10 mM to 90 mM MCP under visible light irradiation for 250 minutes. The degradation increased from 10 mM MCP to 50 mM MCP and decreased when the concentration was increased to 90 mM MCP. 100% of degradation was observed at 75 minutes of visible light irradiation

using 50 mM MCP. 100% degradation was accomplished after 125 minutes of irradiation using 10 mM MCP.

The occurrence of an increased degradation of MG until an optimum concentration could be explained as follows. The degradation of MG was dependent upon the probability of •OH radical formation on the surface of Bi_2O_3 nanoflakes and also the •OH radicals reacting with MG molecules. As the initial concentration of MG increased, more molecules were available for excitation and subsequently its degradation (Mohaghegh et al., 2014; Kumawat, Bhati and Ameta, 2012). In addition, an increasing concentration of MG increases the probability of collision between MG molecules and Bi_2O_3 nanoflakes (Puentes-Cárdenas et al., 2016; Hassan and Hameed, 2011). This could contribute towards the improved degradation of MG. When the optimum concentration was reached, the reduction in MG degradation was attributed towards the increased MG molecules within the system. As the Bi_2O_3 surface area was fixed, only limited number of dye molecules could attach on the active sites of the Bi_2O_3 nanoflakes causing the remainder molecules to persist in the solution until the pre-attached molecules have been degraded (Khemani, Srivastava and Srivastava, 2011). Another factor contributing to the decrease in degradation efficiency is the decrease in light penetration through the MG solution as large quantities of MG molecules shielded the fluorescent light from reaching the surface of Bi_2O_3. According to the Beer-Lambert law, the path length of photons entering the solution decreased and caused a lower photon absorption on Bi_2O_3 nanoflakes. In turn, it inhibited the separation of the e^--h^+ pair, reducing the production of •OH radicals. (Nezamzadeh-Ejhieh and Shahriari, 2011).

4.3.3 Effect of solution pH

The effect of pH on the degradation of MG was investigated by varying the pH of the solution while all other parameters were kept constant. Figure 4.10 displays the MG degradation by varying the solution pH. At an acidic pH 3, the degradation of MG was recorded to be 18.2% while an increase in pH to its natural pH 6 observed a 100% degradation of MG within 20 minutes. A similar result was also observed for

pH 7. The minor difference between the degradation of MG could be seen at the 15 minute mark whereby the degradation for pH 6 was found to be at 62.2% while it was 55.8% for pH 7. Further increase in pH value to pH 10 recorded a decrease in degradation in which 25.9% of MG was degraded. This proved that both pH 6 and pH 7 showed a comparable degradation effectiveness on the degradation of MG.

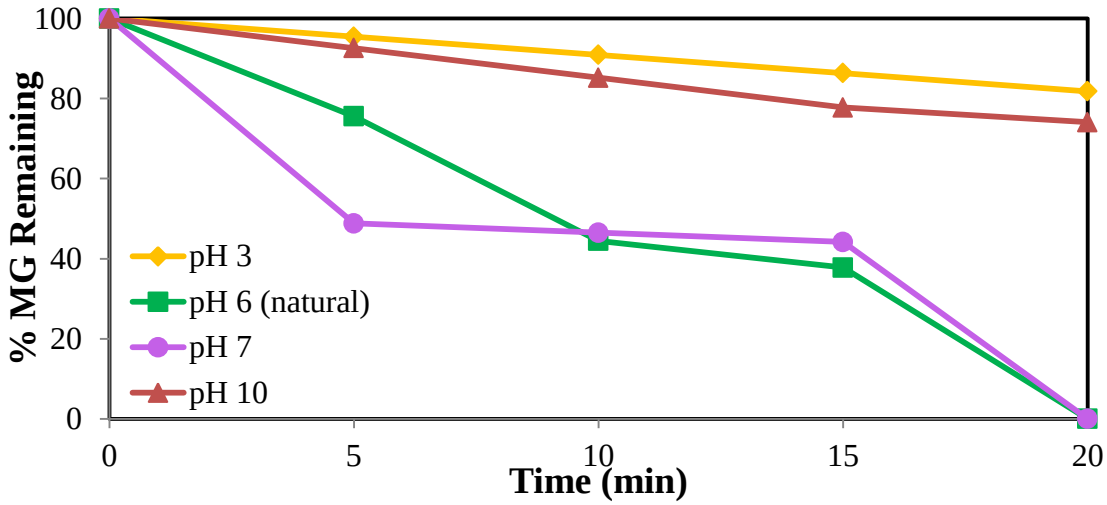

Figure 4.10: Effect of various pH on the degradation of MG in the presence of 10 mM H_2O_2 ([MG] = 5 mg/L ; photocatalyst loading = 1 g/L).

The influence of pH has been related to the surface charge of the photocatalyst and could be explained based on the point zero charge (pzc). The point zero charge was where the surface of the photocatalyst was understood to be uncharged at a certain pH value (Chen and Lu, 2007). Above and below this value, the photocatalyst was either negatively or positively charged.

At an acidic pH 3, the pH was noted to be below the pzc of Bi_2O_3 which was 4.6 (Sood et al., 2015). When the pH of the solution was lesser than 4.6, the surface of Bi_2O_3 nanoflakes became positively charged. The ionization state on the surface of a photocatalyst could be protonated under acidic conditions. It was noted by Fu et al. (2008) that the dissolution of Bi_2O_3 into $BiOH_2^+$ could occur within an acidic medium. This protonated group repelled the similarly positive charge of MG. The cationic MG was unable to be adsorbed onto the surface of the photocatalyst to undergo degradation.

On the other hand, pH 6 and 7 showed exceptional photocatalytic degradation of MG. As these pHs were above the pzc of Bi_2O_3, the surface charge of Bi_2O_3 was negatively charged. This promoted the attraction of the positively charged MG molecules onto the surface of Bi_2O_3 nanoflakes. In addition, a slightly alkaline medium encouraged the production of •OH radicals as more OH^- ions were present in the system to be converted. However, at a very high pH (pH 10), competition between the excessive OH^- and dye molecules existed for the active sites on the surface of Bi_2O_3 nanoflakes (Rajabi and Farsi, 2015; Rajabi et al., 2013). As a result, the formation of the reactive •OH radicals and the degradation of MG were affected as the quantity of active sites on the nanoflakes were greatly reduced.

As mentioned in Ejhieh and Khorsandi (2010) and Kasiri, Aleboyeh and Aleboyeh (2008), in an acidic medium, the acidification of the solution through the addition of HCl induced a high amount of conjugate base into the solution. Upon dissociation, the anionic Cl^- was able to react with the available •OH radicals which lead towards the formation of inorganic radical ions ($ClO^{-\bullet}$). The $ClO^{-\bullet}$ ions exhibit a much lower reactivity (1.49 eV) than •OH and hence do not partake in the degradation of MG.

On the contrary, in alkaline pHs, the presence of huge quantities of OH^- ions caused the formation of more •OH radicals which enhanced the degradation of MG significantly (Nezamzadeh-Ejhieh and Shahriari, 2011). MG is a cationic dye that is positively charged due to the ionization of the ammonium groups in water. Its electrostatic attraction onto the surface of the photocatalyst is favorable within basic solutions and weak in acidic solutions. At highly alkaline pHs, the excess OH^- competes with the MG molecules for the active sites on the photocatalyst.

It was shown that various parameters such as H_2O_2 concentration, initial MG concentration and solution pH played an important role in the degradation of MG. The addition of an oxidizing agent, at 10 mM H_2O_2 exhibited an improved degradation of MG within 20 minutes of fluorescent light irradiation. The variation between initial MG concentrations depicted an enhanced degradation of MG until 5 mg/L and this was determined to be its best concentration. Finally, the study conducted on the effects of pH on the degradation of MG revealed the great influence of the solution pH on the surface charge of the Bi_2O_3 nanoflakes. It was

found that the natural pH 6 showed and efficient degradation of MG. The combined parameters enabled the complete degradation of MG dye in 20 minutes of irradiation.

4.4 Mineralization study

Figure 4.11 shows the variation of MG in terms of photocatalytic degradation and COD efficiency in the presence of Bi_2O_3 nanoflakes. As indicated, MG was photocatalytically degraded by 100% within the first 20 minutes under fluorescent light irradiation whereas the maximum COD reduction observed after 20 minutes of irradiation was approximately 65%. The percentage COD reduction was then observed to decrease as the time increased up to 80 minutes in which 81% of COD was reduced.

The results obtained were in accordance to those produced by Saikia et al. (2015), Vignesh, Rajarajan and Suganthi (2014) and Zhang et al. (2013). Saikia et al. using ZnO as the photocatalyst managed to obtain 100% degradation of Malachite Green under 100 minutes of UV light irradiation while obtaining 90.8% COD reduction under similar duration. Vignesh, Rajarajan and Suganthi achieved 93% of MB degradation under 180 minutes of visible light irradiation using Ni and Th co-doped ZnO nanoparticles. Under the same 180 minutes, only 70% of COD was reduced. Zhang et al. used a novel BiOCl thin film as their photocatalyst and have recorded 98% degradation under UV light irradiation for 8 hours while obtained a 73.47% COD reduction.

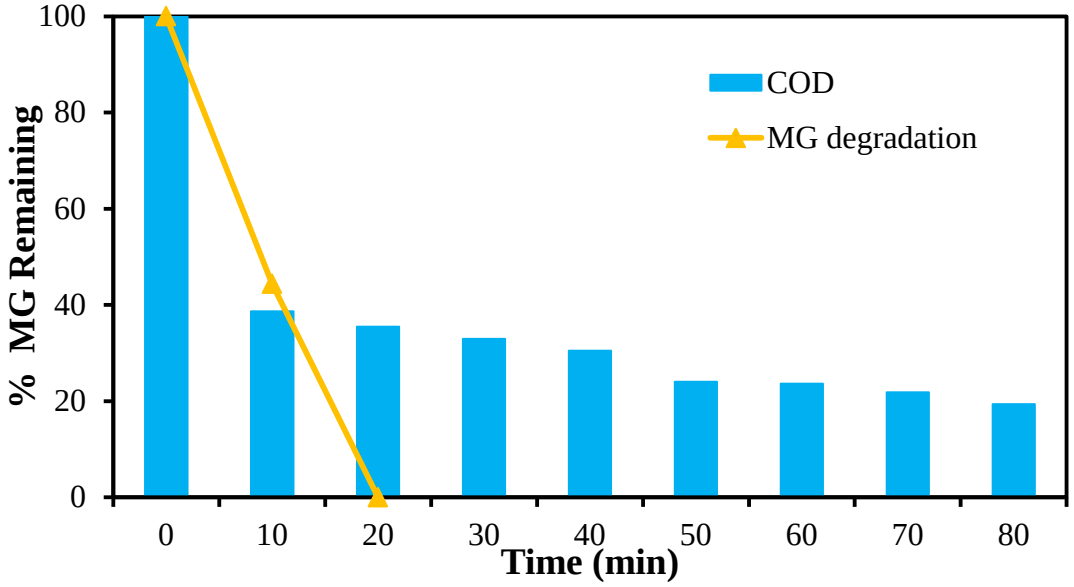

Figure 4.11: Variations of MG and COD efficiency in the presence of Bi_2O_3 nanoflakes ([MG] = 5 mg/L; photocatalyst loading = 1 g/L; [H_2O_2] = 10 mM; solution pH = 7).

According to Divya, Bansal and Jana (2013) and Rauf and Ashraf (2009), during the photocatalytic degradation, the production of •OH radicals enabled the oxidation or reduction via h^+ or e^- of the azo bonds that held the colour of the dye. These cleavages of the bonds lead to the degradation of MG. When the azo bonds were broken down, they in turn produced a more stable transformation by-products or intermediates. It was confirmed by Mai et al. (2008) that there were 32 identified colourless intermediates of MG that were formed under 12 hours of visible light irradiation. The photocatalytic degradation managed to degrade the smaller organic molecules that were formed during the initial stages of degradation, leaving behind the less decomposable by-products. As a result, the decrease in COD percentage would take a longer time to be achieved compared to the photocatalytic degradation of the MG.

4.5 Various dye degradation studies

In order to determine the feasibility of Bi_2O_3 nanoflakes, they were experimented in the treatment of various dyes such as MG, MB and RhB and their photocatalytic degradation were tested in the presence of H_2O_2. Herein, the dyes were degraded under previously optimized conditions with the presence of 10 mM H_2O_2, initial dye concentration of 5.0 mg/L and pH 7. Figure 4.12 illustrates the photocatalytic degradation of various dyes using Bi_2O_3 nanoflakes. MB was shown to possess a better degradation as compared to RhB. Upon 20 minutes of fluorescent irradiation, 69.9% of MB was degraded while 42.4% of RhB was degraded. In comparison, the optimized conditions enabled 100% MG degradation within 20 minutes. The degradation efficiency followed the order of MG > MB > RhB.

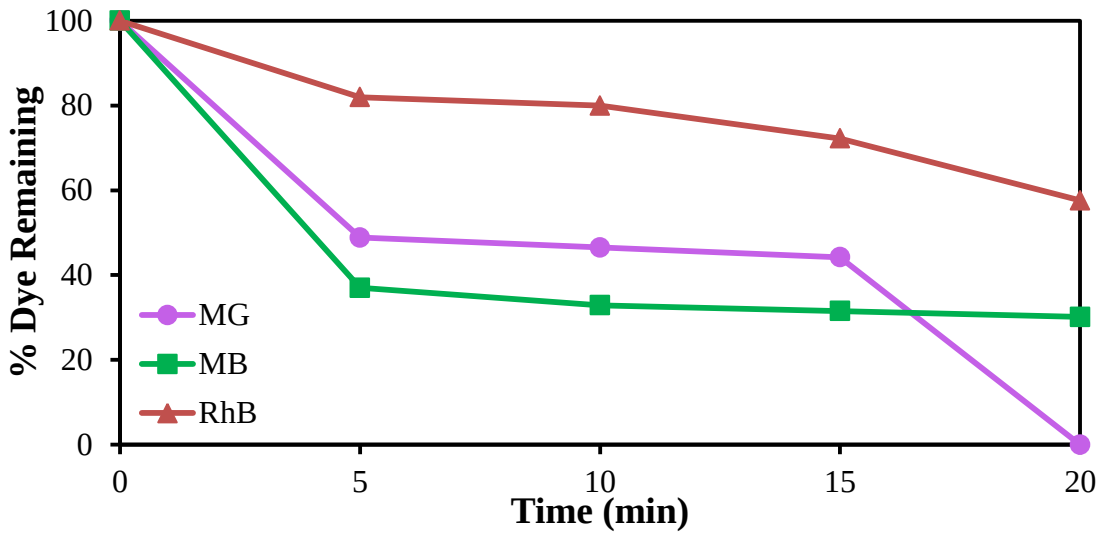

Figure 4.12: Photocatalytic degradation of various dyes using Bi_2O_3 nanoflakes containing 10 mM of H_2O_2 ([dye] = 5 mg/L; photocatalyst loading = 1 g/L; solution pH = 7).

Similar results were obtained by Hashemzadeh, Rahimi and Gaffarinejad (2013) whereby the photocatalytic degradation of MB was higher than RhB. Several factors could be linked to the degradation efficiency of MB and RhB. The enhanced degradation of MB over RhB could be attributed towards the complex molecular structure of RhB making it less degradable. In the process of adsorption of dye molecules, the presence of diethylamine group in MB made it less negative than RhB

as the carboxylic acid group in RhB made it more negatively charged, hence a strong repulsion by the negatively charged Bi_2O_3 nanoflake surface (Natarajan, Bajaj and Tayade, 2014). This strong repulsion could have led towards a lower degradation of RhB.

Hashemzadeh, Rahimi and Gaffarinejad (2013) proposed that the inefficient degradation of RhB was contributed to its functional group. Functional groups that tend to decrease the solubility of the molecules in water decreases the degradation process (Muhd Julkapli, Bagheri and Bee Abd Hamid, 2014). RhB with two longer side groups (diethylamino) compared to the two shorter side groups (dimethylamino) of MB increased the hydrophobicity of the dye molecules.

The synthesized Bi_2O_3 nanoflakes showed different degradations of different pollutants. However, it was demonstrated that it could enhance the degradation of the various pollutants such as MB and RhB because of its photocatalytic ability. It contributed towards the practicality of the synthesized Bi_2O_3 nanoflakes as it could be applied in the degradation of other organic pollutants.

CHAPTER 5

CONCLUSION AND RECOMMENDATIONS

5.1 Conclusion

In summary, Bi_2O_3 nanoflakes were successfully synthesized via a co-precipitation route using cetyltrimethyl ammonium bromide (CTAB) as a surfactant. The synthesized photocatalyst was characterized using XRD, FESEM-EDX and UV-Vis DRS analyses. The XRD analysis proved that the synthesized Bi_2O_3 photocatalyst was of the α-monoclinic phase and possessed high crystallinity. FESEM showed the surface morphology of the photocatalyst and it was determined to be a nanoflake structure with an average length of 250 nm and 60 nm thickness. In addition, the EDX analysis confirmed that the synthesized Bi_2O_3 was mainly composed of Bi and O elements with its atomic percent being 23.13% Bi and 76.87% O. The UV-Vis DRS enabled the band gap energy measurement of Bi_2O_3. This was calculated to be 2.95 eV. This meant that the photocatalyst can be activated under visible light irradiation.

A comparison study was conducted using Bi_2O_3 nanoflakes, commercial Bi_2O_3 and TiO_2 in the presence of H_2O_2. It was found that the as-synthesized Bi_2O_3 nanoflakes exhibited superior photocatalytic activity compared to both commercial Bi_2O_3 and TiO_2. The photodegradation achieved for commercial Bi_2O_3 and TiO_2 were 79% and 68% of MG under 30 minutes of fluorescent light irradiation respectively while the as-synthesized nanoflakes achieved 100% degradation in 20 minutes. In addition, a sedimentation test was carried out to assess the ease of removal of the Bi_2O_3 nanoflakes from the solution. It was proven that within 30 minutes, the nanoflakes were able to settle and formed a layer at the bottom while the

comparison TiO_2 was unable to settle within 30 minutes. This feature allows for the reusability of the photocatalyst in the wastewater treatment industry.

Under fluorescent light irradiation, several parameters were tested including the effects of H_2O_2 concentration, initial dye concentration and also pH for the degradation of MG. Under optimized conditions, 100% degradation of MG was achieved within 20 minutes of fluorescent light irradiation. A COD analysis was also conducted to determine the mineralization extent of the photocatalyst under optimized experimental conditions. A longer time was taken in order to achieve a complete mineralization of MG. 81% of COD decrease was obtained under 80 minutes of irradiation.

Various dye degradation using MG, MB and RhB in the presence of Bi_2O_3 nanoflakes was also examined under optimized conditions. It was discovered that the photocatalytic degradation efficiency was MG > MB > RhB. This showed that the as-synthesized photocatalyst exhibited a wide suitability in the visible light photocatalytic activity of organic pollutants in the presence of H_2O_2.

5.2 Recommendations

Upon completion of the present study, several fundamental aspects should be paid attention to in future photocatalytic studies.

1. The study could be given focus on synthesizing a 3D and porous Bi_2O_3 structure as they are able to enhance the adsorption of organic pollutants.
2. The synthesized photocatalyst should be tested using solar light irradiation as the light source. As solar light is an abundant, free and clean source it would be beneficial for the photocatalysis technology.
3. Bi_2O_3 photocatalytic ability should be tested using real textile wastewater as mixtures of dyes are present in the wastewater.

REFERENCES

Abbas, I. and Zaheer, S. (2014). Advanced oxidation process for wastewater treatment: A review. *American International Journal of Research in Science, Technology, Engineering & Mathematics*, 7, pp. 189-191.

Abid, M., Zablouk, M. and Abid-Alameer, A. (2012). Experimental study of dye removal from industrial wastewater by membrane technologies of reverse osmosis and nanofiltration. *Iranian Journal of Environmental Health Science & Engineering*, 9, pp. 1-9.

Abo-Farha, S. (2010). Photocatalytic degradation of monoazo and diazo dyes in wastewater on nanometer-sized TiO_2. *Journal of American Science*, 6, pp. 130-142.

Adhikari, S., Zhang, L., Gross, M. and Lachgar, A. (2015). Enhancement of visible light photocatalytic activity of tantalum oxynitride and tantalum nitride by coupling with bismuth oxide; an example of composite photocatalysis. In: *2014 MRS Fall Meeting*. [online] MRS Proceedings. Available at: http://10.1557/opl.2015.194 [Accessed 15 Feb. 2016].

Akpan, U. and Hameed, B. (2009). Parameters affecting the photocatalytic degradation of dyes using TiO_2-based photocatalysts: A review. *Journal of Hazardous Materials*, 170, pp. 520-529.

Al-Kadhemy, M., Alsharuee, I. and Al-Zuky, A. (2011). Analysis of the effect of the concentration of Rhodamine B in ethanol on the fluorescence spectrum using the "Gauss Mod" function. *Journal of Physical Science*, 22, pp. 77–86.

Ambreen, S., Pandey, N., Mayer, P. and Pandey, A. (2014). Characterization and photocatalytic study of tantalum oxide nanoparticles prepared by the hydrolysis of

tantalum oxo-ethoxide $Ta_8(\mu_3\text{-}O)_2(\mu\text{-}O)_8(\mu\text{-}OEt)_6(OEt)_{14}$. *Beilstein Journal of Nanotechnology*, 5, pp. 1082-1090.

Ameta, A., Ameta, R. and Ahuja, M. (2013). Photocatalytic degradation of methylene blue over ferric tungstate. *Scientific Reviews and Chemical Communications*, 3, pp. 172-180.

Anandan, S. and Wu, J. (2009). Microwave assisted rapid synthesis of Bi_2O_3 short nanorods. *Materials Letters*, 63, pp. 2387-2389.

Anandan, S., Lee, G., Chen, P., Fan, C. and Wu, J. (2010). Removal of orange II dye in water by visible light assisted photocatalytic ozonation using Bi_2O_3 and Au/Bi_2O_3 nanorods. *Industrial & Engineering Chemistry Research*, 49, pp. 9729-9737.

Ananpattarachai, J., Kajitvichyanukul, P. and Seraphin, S. (2009). Visible light absorption ability and photocatalytic oxidation activity of various interstitial N-doped TiO_2 prepared from different nitrogen dopants. *Journal of Hazardous Materials*, 168, pp. 253-261.

Asenjo, N., Santamaría, R., Blanco, C., Granda, M., Álvarez, P. and Menéndez, R. (2013). Correct use of the Langmuir–Hinshelwood equation for proving the absence of a synergy effect in the photocatalytic degradation of phenol on a suspended mixture of titania and activated carbon. *Carbon*, 55, pp. 62-69.

Atalay, S. and Ersöz, G. (2015). Advanced oxidation processes for removal of dyes from aqueous media. *Green Chemistry for Dyes Removal from Wastewater*, pp. 83-117.

Avasarala, B., Tirukkovalluri, S. and Bojja, S. (2010). Synthesis, characterization and photocatalytic activity of alkaline earth metal doped titania. *Indian Journal of Chemistry: Section A*, 49, pp. 1189-1196.

Barka, N., Bakas, I., Qourzal, S. and Ait-Ichou, A. (2013). Degradation of phenol in water by titanium dioxide photocatalysis. *Oriental Journal of Chemistry*, 29, pp. 1055-1060.

Barrera-Mota, K., Bizarro, M., Castellino, M., Tagliaferro, A., Hernández, A. and Rodil, S. (2015). Spray deposited β-Bi_2O_3 nanostructured films with visible photocatalytic activity for solar water treatment. *Photochemical and Photobiological Sciences*, 14, pp. 1110-1119.

Bazkiaei, Z. and Giahi, M. (2016). Photocatalytic degradation of an anionic surfactant by TiO_2 nanoparticle under UV radiation in aqueous solutions. *Journal of Physical & Theoretical Chemistry*, 13, pp. 1-8.

Bel Hadjltaief, H., Omri, A., Ben Zina, M., Da Costa, P. and Galvez, M. (2015). Titanium dioxide supported on different porous materials as photocatalyst for the degradation of methyl green in wastewaters. *Advances in Materials Science and Engineering*, 2015, pp. 1-10.

Belessi, V., Romanos, G., Boukos, N., Lambropoulou, D. and Trapalis, C. (2009). Removal of Reactive Red 195 from aqueous solutions by adsorption on the surface of TiO_2 nanoparticles. *Journal of Hazardous Materials*, 170, pp. 836-844.

Belgiorno, V. and Rizzo, L. (2012). Emerging contaminants into the environment: contamination pathways and control. 1st ed. [ebook] Fisciano: ASTER, p.113. Available at: https://books.google.com.my/books?isbn=1471076067 [Accessed 1 Aug. 2016].

Benhebal, H., Chaib, M., Salmon, T., Geens, J., Leonard, A., Lambert, S., Crine, M. and Heinrichs, B. (2013). Photocatalytic degradation of phenol and benzoic acid using zinc oxide powders prepared by the sol–gel process. *Alexandria Engineering Journal*, 52, pp. 517-523.

Biçer, M. and Şişman, İ. (2010). Controlled synthesis of copper nano/microstructures using ascorbic acid in aqueous CTAB solution. *Powder Technology*, 198, pp. 279-284.

Bousnoubra, I., Djebbar, K., Abdessemed, A. and Sehili, T. (2016). Decolorization of methyl green and bromocresol purple in mono and binary systems by photochemical processes: direct UV photolysis, Acetone/UV and H_2O_2/UV. A comparative study. *Desalination and Water Treatment*, pp. 1-16.

Brillas, E. and Martínez-Huitle, C. (2015). Decontamination of wastewaters containing synthetic organic dyes by electrochemical methods. An updated review. *Applied Catalysis B: Environmental*, 166-167, pp. 603-643.

Cabansag, J., Dumelod, J., Alfaro, J., Arsenal, J., Sambot, J., Enerva, L. and Leaño Jr, J. (2013). Photocatalytic degradation of aqueous C.I. reactive violet 5 using bulk zinc oxide (ZnO) slurry. *Philippine Journal of Science*, 142, pp. 77-85.

Chaturvedi, S., Dave, P. and Shah, N. (2012). Applications of nano-catalyst in new era. *Journal of Saudi Chemical Society*, 16, pp. 307-325.

Chen, C. and Lu, C. (2007). Mechanistic studies of the photocatalytic degradation of methyl green: an investigation of products of the decomposition processes. *Environmental Science & Technology*, 41, pp. 4389-4396.

Chen, C., Cao, S., Yu, W., Xie, X., Liu, Q., Tsang, Y. and Xiao, Y. (2015). Adsorption, photocatalytic and sunlight-driven antibacterial activity of Bi_2WO_6/graphene oxide nanoflakes. *Vacuum*, 116, pp. 48-53.

Chen, D., Meng, Y., Zeng, D., Liu, Z., Yu, H. and Zhong, X. (2012). CTAB-assisted low-temperature synthesis of $SrFe_{12}O_{19}$ ultrathin hexagonal platelets and its formation mechanism. *Materials Letters*, 76, pp. 84-86.

Chen, R., Shen, Z., Wang, H., Zhou, H., Liu, Y., Ding, D. and Chen, T. (2011). Fabrication of mesh-like bismuth oxide single crystalline nanoflakes and their visible light photocatalytic activity. *Journal of Alloys and Compounds*, 509, pp. 2588-2596.

Chen, W., Xiao, H., Xu, H., Ding, T. and Gu, Y. (2015). Photodegradation of methylene blue by TiO_2-Fe_3O_4-bentonite magnetic nanocomposite. *International*

Journal of Photoenergy, 2015, pp. 1-7.

Cheng, H., Huang, B., Lu, J., Wang, Z., Xu, B., Qin, X., Zhang, X. and Dai, Y. (2010). Synergistic effect of crystal and electronic structures on the visible-light-driven photocatalytic performances of Bi_2O_3 polymorphs. *Physical Chemistry Chemical Physics.*, 12, pp. 15468-15475.

Cheng, M., Zeng, G., Huang, D., Lai, C., Xu, P., Zhang, C. and Liu, Y. (2016). Hydroxyl radicals based advanced oxidation processes (AOPs) for remediation of soils contaminated with organic compounds: A review. *Chemical Engineering Journal*, 284, pp. 582-598.

Cho, S., Jang, J., Lee, K. and Lee, J. (2014). Research Update: Strategies for efficient photoelectrochemical water splitting using metal oxide photoanodes. *Applied Physics Letters Materials*, 2, pp. 010703

Chu, Y., Lee, G., Chen, C., Ma, S., Wu, J., Horng, T., Chen, K. and Chen, J. (2013). Preparation of bismuth oxide photocatalyst and its application in white-light LEDs. *Journal of Nanomaterials*, 2013, pp. 1-7.

Clarke, E. and Anliker, R. (1980). Organic dyes and pigments. *The Handbook of Environmental Chemistry*, 3, Springer Berlin Heidelberg, pp. 181-215.

Crini, G. (2006). Non-conventional low-cost adsorbents for dye removal: A review. *Bioresource Technology*, 97, pp. 1061-1085.

Daâssi, D., Mechichi, T., Nasri, M. and Rodriguez-Couto, S. (2013). Decolorization of the metal textile dye Lanaset Grey G by immobilized white-rot fungi. *Journal of Environmental Management*, 129, pp. 324-332.

Daghrir, R., Drogui, P. and Robert, D. (2013). Modified TiO_2 for environmental photocatalytic applications: A review. *Industrial & Engineering Chemistry Research*, 52, pp. 3581−3599.

Dalbhanjan, R., Pande, N., Banerjee, B., Hinge, S., Mohod, A. and Gogate, P. (2015). Degradation of patent blue V dye using modified photocatalytic reactor

based on solar and UV irradiations. *Desalination and Water Treatment*, 57, pp. 18217-18228.

Damodar, R., Jagannathan, K. and Swaminathan, T. (2007). Decolourization of reactive dyes by thin film immobilized surface photoreactor using solar irradiation. *Solar Energy*, 81, pp. 1-7.

Daneshvar, N., Ayazloo, M., Khataee, A. and Pourhassan, M. (2007). Biological decolorization of dye solution containing Malachite Green by microalgae *Cosmarium sp. Bioresource Technology*, 98, pp. 1176-1182.

Dawood, S. and Sen, T. (2012). Removal of anionic dye Congo red from aqueous solution by raw pine and acid-treated pine cone powder as adsorbent: Equilibrium, thermodynamic, kinetics, mechanism and process design. *Water Research*, 46, pp. 1933-1946.

de Lasa, H., Serrano, B. and Salaices, M. (2006). *Photocatalytic Reaction Engineering*. 1st ed. [ebook] New York: Springer Science & Business Media, pp. 59-60. Available at: https://books.google.com.my/books?isbn=0387275916 [Accessed 10 Mar. 2016].

de Lima, L., Pereira, L., de Moura, S. and Magalhães, F. (2016). Degradation of organic contaminants in effluents—synthetic and from the textile industry—by fenton, photocatalysis, and H_2O_2 photolysis. *Environmental Science and Pollution Research*, pp. 1-8.

Deng, X., Zhang, Q., Zhao, Q., Ma, L., Ding, M. and Xu, X. (2015). Effects of architectures and H_2O_2 additions on the photocatalytic performance of hierarchical Cu_2O nanostructures. *Nanoscale Research Letters*, 10, pp. 1-9.

Dinesh, G., Anandan, S. and Sivasankar, T. (2016). Synthesis of Fe-doped Bi_2O_3 nanocatalyst and its sonophotocatalytic activity on synthetic dye and real textile wastewater. *Environmental Science and Pollution Research*, pp. 1-11.

Divya, N., Bansal, A. and Jana, A. (2013). Photocatalytic degradation of azo dye orange II in aqueous solutions using copper-impregnated titania. *International Journal of Environmental Science and Technology*, 10, pp. 1265-1274.

Doğar, Ç., Gürses, A., Açıkyıldız, M. and Özkan, E. (2010). Thermodynamics and kinetic studies of biosorption of a basic dye from aqueous solution using green algae *Ulothrix sp. Colloids and Surfaces B: Biointerfaces*, 76, pp. 279-285.

dos Santos, A., Cervantes, F. and van Lier, J. (2007). Review paper on current technologies for decolourisation of textile wastewaters: Perspectives for anaerobic biotechnology. *Bioresource Technology*, 98, pp. 2369-2385.

Ejder-Korucu, M., Gürses, A., Doğar, Ç., Sharma, S. and Açıkyıldız, M. (2015). Removal of organic dyes from industrial effluents: an overview of physical and biotechnological applications. *Green Chemistry for Dyes Removal from Wastewater*, pp. 1-34.

Ejhieh, A. and Khorsandi, M. (2010). Photodecolorization of eriochrome black T using NiS–P zeolite as a heterogeneous catalyst. *Journal of Hazardous Materials*, 176, pp. 629-637.

Elsellami, L., Vocanson, F., Dappozze, F., Puzenat, E., Païsse, O., Houas, A. and Guillard, C. (2010). Kinetic of adsorption and of photocatalytic degradation of phenylalanine effect of pH and light intensity. *Applied Catalysis A: General*, 380, pp. 142-148.

Erkurt, H. (2010). *Biodegradation of azo dyes*. 1st ed. [ebook] Berlin: Springer Science & Business Media, p. 51. Available at: https://books.google.com.my/books?isbn=3642118461 [Accessed 28 Feb. 2016].

Felix, A., Andrew, A. and Mededodec, A. (2014). Heterogeneous photocatalytic degradation of naphthalene using periwinkle shell ash: effect of operating variables, kinetic and isotherm study. *South African Journal of Chemical Engineering*, 19, pp. 31-45.

Foo, K. and Hameed, B. (2010). Decontamination of textile wastewater via TiO_2/activated carbon composite materials. *Advances in Colloid and Interface Science*, 159, pp. 130-143.

Fu, H., Zhang, S., Xu, T., Zhu, Y. and Chen, J. (2008). Photocatalytic degradation of RhB by fluorinated Bi_2WO_6 and distributions of the intermediate products. *Environmental Science & Technology*, 42, pp. 2085-2091.

Gaya, U. and Abdullah, A. (2008). Heterogeneous photocatalytic degradation of organic contaminants over titanium dioxide: A review of fundamentals, progress and problems. *Journal of Photochemistry and Photobiology C: Photochemistry Reviews*, 9, pp. 1-12.

Geethakrishnan, T. and Palanisamy, P. (2006). Degenerate four-wave mixing experiments in methyl green dye-doped gelatin film. *Optik - International Journal for Light and Electron Optics*, 117, pp. 282-286.

Ghaly, A., Ananthashankar, R., Alhattab, M. and Ramakrishnan, V. (2013). Production, characterization and treatment of textile effluents: A critical review. *Journal of Chemical Engineering & Process Technology*, 5, pp. 1-19.

Giménez, S. and Bisquert, J. (2016). *Photoelectrochemical Solar Fuel Production: From Basic Principles to Advanced Devices*. 1st ed. [ebook] Springer, p. 175. Available at: https://books.google.com.my/books?isbn=3319296418 [Accessed 6 Aug. 2016].

Gnanaprakasam, A., Sivakumar, V. and Thirumarimurugan, M. (2015). Influencing parameters in the photocatalytic degradation of organic effluent via nanometal oxide catalyst: A review. *Indian Journal of Materials Science*, 2015, pp. 1-16.

Gogate, P. and Bhosale, G. (2013). Comparison of effectiveness of acoustic and hydrodynamic cavitation in combined treatment schemes for degradation of dye wastewaters. *Chemical Engineering and Processing: Process Intensification*, 71, pp. 59-69.

Guo, J., Zhou, J., Wang, D., Tian, C., Wang, P., Salah Uddin, M. and Yu, H. (2007). Biocalalyst effects of immobilized anthraquinone on the anaerobic reduction of azo dyes by the salt-tolerant bacteria. *Water Research*, 41, pp. 426-432.

Guo, N., Liang, Y., Lan, S., Liu, L., Ji, G., Gan, S., Zou, H. and Xu, X. (2014). Uniform TiO_2–SiO_2 hollow nanospheres: synthesis, characterization and enhanced

adsorption–photodegradation of azo dyes and phenol. *Applied Surface Science*, 305, pp. 562-574.

Gupta, V. and Suhas, (2009). Application of low-cost adsorbents for dye removal: A review. *Journal of Environmental Management*, 90, pp. 2313-2342.

Gupta, V., Jain, R., Agarwal, S., Nayak, A. and Shrivastava, M. (2012). Photodegradation of hazardous dye quinoline yellow catalyzed by TiO_2. *Journal of Colloid and Interface Science*, 366, pp. 135-140.

Hafshejani, M., Ogugbue, C. and Morad, N. (2013). Application of response surface methodology for optimization of decolorization and mineralization of triazo dye Direct Blue 71 by *Pseudomonas aeruginosa*. *3 Biotechnology*, 4, pp. 605-619.

Hajra, P., Shyamal, S., Bera, A., Mandal, H., Sariket, D., Kundu, M., Pande, S. and Bhattacharya, C. (2015). Optimization of Triton-X 100 surfactant in the development of bismuth oxide thin film semiconductor for improved photoelectrochemical water oxidation behavior. *Electrochimica Acta*, 185, pp. 229-235.

Hameed, A., Gombac, V., Montini, T., Felisari, L. and Fornasiero, P. (2009). Photocatalytic activity of zinc modified Bi_2O_3. *Chemical Physics Letters*, 483, pp. 254-261.

Hameed, A., Montini, T., Gombac, V. and Fornasiero, P. (2008). Surface phases and photocatalytic activity correlation of Bi_2O_3/Bi_2O_4-x nanocomposite. *Journal of American Chemical Society*, 130, pp. 9658-9659.

Hao, W., Gao, Y., Jing, X., Zou, W., Chen, Y. and Wang, T. (2014). visible light photocatalytic properties of metastable γ-Bi_2O_3 with different morphologies. *Journal of Materials Science & Technology*, 30, pp. 192-196.

Hariharan, S., Udayabhaskar, R., Ravindran, T. and Karthikeyan, B. (2016). Surfactant assisted control on optical, fluorescence and phonon lifetime in α-Bi_2O_3 microrods. *Spectrochimica Acta Part A: Molecular and Biomolecular Spectroscopy*, 163, pp. 13-19.

Hashemzadeh, F., Rahimi, R. and Gaffarinejad,, A. (2013). Photocatalytic degradation of methylene blue and rhodamine B dyes by niobium oxide nanoparticles synthesized via hydrothermal method. *International Journal of Applied Chemical Sciences Research*, 1, pp. 95-102.

Hassan, H. and Hameed, B. (2011). Fenton-like oxidation of acid red 1 solutions using heterogeneous catalyst based on ball clay. *International Journal of Environmental Science and Development*, 2, pp. 218-222.

Hay, S., Obee, T., Luo, Z., Jiang, T., Meng, Y., He, J., Murphy, S. and Suib, S. (2015). The viability of photocatalysis for air purification. *Molecules*, 20, pp. 1319-1356.

He, R., Cao, S., Zhou, P. and Yu, J. (2014). Recent advances in visible light Bi-based photocatalysts. *Chinese Journal of Catalysis*, 35, pp.989-1007.

Ho, C., Chan, C., Huang, Y., Tien, L. and Chao, L. (2013). The study of optical band edge property of bismuth oxide nanowires α-Bi_2O_3. *Optics Express*, 21, pp. 11965-11972.

Hosseini Koupaie, E., Alavi Moghaddam, M. and Hashemi, S. (2011). Post-treatment of anaerobically degraded azo dye Acid Red 18 using aerobic moving bed biofilm process: Enhanced removal of aromatic amines. *Journal of Hazardous Materials*, 195, pp. 147-154.

Hou, J., Yang, C., Wang, Z., Zhou, W., Jiao, S. and Zhu, H. (2013). In situ synthesis of α–β phase heterojunction on Bi_2O_3 nanowires with exceptional visible-light photocatalytic performance. *Applied Catalysis B: Environmental*, 142-143, pp. 504-511.

Hsieh, C., Fan, W., Chen, W. and Lin, J. (2009). Adsorption and visible-light-derived photocatalytic kinetics of organic dye on Co-doped titania nanotubes prepared by hydrothermal synthesis. *Separation and Purification Technology*, 67, pp. 312-318.

Hsieh, S., Lee, G., Chen, C., Chen, J., Ma, S., Horng, T., Chen, K. and Wu, J. (2012). Synthesis of Pt doped Bi_2O_3/RuO_2 photocatalysts for hydrogen production from water splitting using visible light. *Journal of Nanoscience and Nanotechnology*, 12, pp. 5930-5936.

Huang, Q., Zhang, S., Cai, C. and Zhou, B. (2011). β- and α-Bi_2O_3 nanoparticles synthesized via microwave-assisted method and their photocatalytic activity towards the degradation of Rhodamine B. *Materials Letters*, 65, pp. 988-990.

Hunger, K. (2007). *Industrial dyes: chemistry, properties, applications*. 1st ed. [ebook] John Wiley & Sons, pp. 2-4. Available at: https://books.google.com.my/books?isbn=3527606068 [Accessed 28 Feb. 2016].

Iljinas, A. and Marcinauskas, L. (2015). Formation of bismuth oxide nanostructures by reactive plasma assisted thermal evaporation. *Thin Solid Films*, 594, pp. 192-196.

Iyyapushpam, S., Nishanthi, S. and Pathinettam Padiyan, D. (2012). Synthesis of room temperature bismuth oxide and its photocatalytic activity. *Materials Letters*, 86, pp. 25-27.

Iyyapushpam, S., Nishanthi, S. and Pathinettam Padiyan, D. (2013). Photocatalytic degradation of methyl orange using α-Bi_2O_3 prepared without surfactant. *Journal of Alloys and Compounds*, 563, pp. 104-107.

Jakab, A., Colar, L., Pode, R., Cocheci, L. and Manea, F. (2012). Catalytic photodegradation and mineralization of cationic dye methylene blue from aqueous solution onto copper doped zeolite. *Revista De Chimie*, 63, pp. 1016-1022.

Jalalah, M., Faisal, M., Bouzid, H., Park, J., Al-Sayari, S. and Ismail, A. (2015). Comparative study on photocatalytic performances of crystalline α- and β-Bi_2O_3 nanoparticles under visible light. *Journal of Industrial and Engineering Chemistry*, 30, pp. 183-189.

Jiang, H., Dai, H., Xia, Y. and He, H. (2010). Synthesis and characterization of wormhole-like mesoporous SnO_2 with high surface area. *Chinese Journal of Catalysis*, 31, pp. 295-301.

Kagalkar, A., Jagtap, U., Jadhav, J., Bapat, V. and Govindwar, S. (2009). Biotechnological strategies for phytoremediation of the sulfonated azo dye Direct Red 5B using Blumea malcolmii Hook. *Bioresource Technology*, 100, pp. 4104-4110.

Kamalakkannan, J., Chandraboss, V., Karthikeyan, B. and Senthilvelan, S. (2016). Synthesis of $InMoO_3$–TiO_2 nanocomposite – photocatalysis of genotoxic dye multiapplication study. *Ceramics International*, 42, pp. 10197-10208.

Karnan, T. and Samuel, S. (2016). A novel bio-mimetic approach for the fabrication of Bi_2O_3 nanoflakes from rambutan (Nephelium lappaceum L.) peel extract and their photocatalytic activity. *Ceramics International*, 42, pp. 4779-4787.

Karthikeyan, B., Udayabhaskar, R. and Kishore, A. (2014). Optical and phonon properties of Sm-doped α-Bi_2O_3 microrods. *Applied Physics A*, 117, pp. 1409-1414.

Kasiri, M., Aleboyeh, H. and Aleboyeh, A. (2008). Degradation of acid blue 74 using Fe-ZSM5 zeolite as a heterogeneous photo-fenton catalyst. *Applied Catalysis B: Environmental*, 84, pp. 9-15.

Khandare, R. and Govindwar, S. (2015). Phytoremediation of textile dyes and effluents: Current scenario and future prospects. *Biotechnology Advances*, 33, pp. 1697-1714.

Khataee, A. and Kasiri, M. (2010). Photocatalytic degradation of organic dyes in the presence of nanostructured titanium dioxide: Influence of the chemical structure of dyes. *Journal of Molecular Catalysis A: Chemical*, 328, pp. 8-26.

Khataee, A., Pons, M. and Zahraa, O. (2009). Photocatalytic degradation of three azo dyes using immobilized TiO_2 nanoparticles on glass plates activated by UV light

irradiation: Influence of dye molecular structure. *Journal of Hazardous Materials*, 168, pp. 451-457.

Khemani, L., Srivastava, M. and Srivastava, S. (2011). *Chemistry of Phytopotentials: Health, Energy and Environmental Perspectives*. 1st ed. [ebook] Springer Science & Business Media, p. 209. Available at: https://books.google.com.my/books?isbn=3642233945 [Accessed 7 Aug. 2016].

Khezrianjoo, S. and Revanasiddappa, H. (2012). Langmuir-Hinshelwood kinetic expression for the photocatalytic degradation of Metanil Yellow aqueous solutions by ZnO catalyst. *Chemical Sciences Journal*, 2012, pp. 1-7.

Klavarioti, M., Mantzavinos, D. and Kassinos, D. (2009). Removal of residual pharmaceuticals from aqueous systems by advanced oxidation processes. *Environment International*, 35, pp. 402-417.

Konstantinou, I. and Albanis, T. (2004). TiO_2-assisted photocatalytic degradation of azo dyes in aqueous solution: kinetic and mechanistic investigations. *Applied Catalysis B: Environmental*, 49, pp. 1-14.

Kumawat, R., Bhati, I. and Ameta, R. (2012). Role of some metal ions in photocatalytic degradation of rose bengal dye. *Indian Journal of Chemical Technology*, 19, pp. 191-194.

Lam, S.M, Sin, J.C, Abdullah, A.Z. and Mohamed, A.R. (2012). Degradation of wastewaters containing organic dyes photocatalysed by zinc oxide: a review. *Desalination and Water Treatment*, 41, pp. 131-169.

Lam, S.M, Sin, J.C. and Mohamed, A. (2010). Recent patents on photocatalysis over nanosized titanium dioxide. *CHENG*, 1, pp. 209-219.

Leontie, L., Caraman, M., Visinoiu, A. and Rusu, G. (2005). On the optical properties of bismuth oxide thin films prepared by pulsed laser deposition. *Thin Solid Films*, 473, pp. 230-235.

Li, F., Sun, S., Jiang, Y., Xia, M., Sun, M. and Xue, B. (2008). Photodegradation of an azo dye using immobilized nanoparticles of TiO_2 supported by natural porous mineral. *Journal of Hazardous Materials*, 152, pp. 1037-1044.

Li, J., Sun, F., Gu, K., Wu, T., Zhai, W., Li, W. and Huang, S. (2011). Preparation of spindly CuO micro-particles for photodegradation of dye pollutants under a halogen tungsten lamp. *Applied Catalysis A: General*, 406, pp. 51-58.

Lu, Y., Zhao, Y., Zhao, J., Song, Y., Huang, Z., Gao, F., Li, N. and Li, Y. (2015). Induced aqueous synthesis of metastable β-Bi_2O_3 microcrystals for visible-light photocatalyst study. *Crystal Growth & Design*, 15, pp. 1031-1042.

Ma, J., Zhang, L., Wang, Y., Lei, S., Luo, X., Chen, S., Zeng, G., Zou, J., Luo, S. and Au, C. (2014). Mechanism of 2,4-dinitrophenol photocatalytic degradation by ζ-Bi_2O_3/Bi_2MoO_6 composites under solar and visible light irradiation. *Chemical Engineering Journal*, 251, pp. 371-380.

Magalhães, P., Ângelo, J., Sousa, V., Nunes, O., Andrade, L. and Mendes, A. (2015). Synthesis and assessment of a graphene-based composite photocatalyst. *Biochemical Engineering Journal*, 104, pp. 20-26.

Mai, F., Chen, C., Chen, J. and Liu, S. (2008). Photodegradation of methyl green using visible irradiation in ZnO suspensions. *Journal of Chromatography A*, 1189, pp. 355-365.

Mai, F., Lu, C., Wu, C., Huang, C., Chen, J. and Chen, C. (2008). Mechanisms of photocatalytic degradation of Victoria Blue R using nano-TiO_2. *Separation and Purification Technology*, 62, pp. 423-436.

Malik, A. and Grohmann, E. (2011). *Environmental Protection Strategies for Sustainable Development*. 1st ed. [ebook] Springer Science & Business Media, pp. 19. Available at: https://books.google.com.my/books?isbn=9400715919 [Accessed 19 Mar. 2016].

Mandal, N. (2014). Performance of low-cost bio adsorbents for the removal of metal ions – A review. *International Journal of Science and Research (IJSR)*, 3, pp. 177-180.

Martínez-de la Cruz, A. and Obregón Alfaro, S. (2009). Synthesis and characterization of nanoparticles of α-$Bi_2Mo_3O_{12}$ prepared by co-precipitation method: Langmuir adsorption parameters and photocatalytic properties with Rhodamine B. *Solid State Sciences*, 11, pp. 829-835.

Martirosyan, K., Wang, L., Vicent, A. and Luss, D. (2009). Synthesis and performance of bismuth trioxide nanoparticles for high energy gas generator use. *Nano Science and Technology Institute-Nanotechnology*, 1, pp. 82-85.

Mehring, M. (2007). From molecules to bismuth oxide-based materials: Potential homo- and heterometallic precursors and model compounds. *Coordination Chemistry Reviews*, 251, pp. 974-1006.

Merouani, S., Hamdaoui, O., Saoudi, F. and Chiha, M. (2010). Sonochemical degradation of Rhodamine B in aqueous phase: Effects of additives. *Chemical Engineering Journal*, 158, pp. 550-557.

Meziti, C. and Boukerroui, A. (2012). Removal of a basic textile dye from aqueous solution by adsorption on regenerated clay. *Procedia Engineering*, 33, pp. 303-312.

Milenova, K., Stambolova, I., Blaskov, V., Eliyas, A., Vassilev, S. and Shipochka, M. (2013). The effect of introducing copper dopant on the photocatalytic activity of ZnO nanoparticles. *Journal of Chemical Technology and Metallurgy*, 48, pp. 259-264.

Modirshahla, N., Behnajady, M. and Jangi Oskui, M. (2009). Investigation of the efficiency of ZnO photocatalyst in the removal of p-nitrophenol from contaminated water. *Iranian Journal of Chemistry and Chemical Engineering (IJCCE)*, 28, pp. 49-55.

Mohaghegh, N., Tasviri, M., Rahimi, E. and Gholami, M. (2014). Nano sized ZnO composites: preparation, characterization and application as photocatalysts for degradation of AB92 azo dye. *Materials Science in Semiconductor Processing*, 21, pp. 167-179.

Mousa, M., Bayoumy, W. and Khairy, M. (2013). Characterization and photo-chemical applications of nano-ZnO prepared by wet chemical and thermal decomposition methods. *Materials Research Bulletin*, 48, pp. 4576-4582.

Muhd Julkapli, N., Bagheri, S. and Bee Abd Hamid, S. (2014). Recent advances in heterogeneous photocatalytic decolorization of synthetic dyes. *The Scientific World Journal*, 2014, pp. 1-25.

Naddeo, V., Rizzo, L. and Belgiorno, V. (2011). *Water, Wastewater and Soil Treatment by Advanced Oxidation Processes*. 1st ed. [ebook] Fisciano: Lulu.com, p. 14. Available at: https://books.google.com.my/books?isbn=1446129675 [Accessed 22 Mar. 2016].

Nataraj, S., Hosamani, K. and Aminabhavi, T. (2009). Nanofiltration and reverse osmosis thin film composite membrane module for the removal of dye and salts from the simulated mixtures. *Desalination*, 249, pp. 12-17.

Natarajan, T., Bajaj, H. and Tayade, R. (2014). Preferential adsorption behavior of methylene blue dye onto surface hydroxyl group enriched TiO_2 nanotube and its photocatalytic regeneration. *Journal of Colloid and Interface Science*, 433, pp. 104-114.

Nezamzadeh-Ejhieh, A. and Amiri, M. (2013). CuO supported Clinoptilolite towards solar photocatalytic degradation of p-aminophenol. *Powder Technology*, 235, pp. 279-288.

Nezamzadeh-Ejhieh, A. and Shahriari, E. (2011). Heterogeneous photodecolorization of Methyl Green catalyzed by Fe(II)-o-Phenanthroline/Zeolite Y nanocluster. *International Journal of Photoenergy*, 2011, pp. 1-10.

Nezamzadeh-Ejhieh, A. and Shams-Ghahfarokhi, Z. (2013). Photodegradation of methyl green by nickel-dimethylglyoxime/ZSM-5 zeolite as a heterogeneous catalyst. *Journal of Chemistry*, 2013, pp. 1-11.

Ogata, F., Imai, D. and Kawasaki, N. (2015). Cationic dye removal from aqueous solution by waste biomass produced from calcination treatment of rice bran. *Journal of Environmental Chemical Engineering*, 3, pp. 1476-1485.

Oudghiri-Hassani, H., Rakass, S., Al Wadaani, F., Al-ghamdi, K., Omer, A., Messali, M. and Abboudi, M. (2015). Synthesis, characterization and photocatalytic activity of α-Bi_2O_3 nanoparticles. *Journal of Taibah University for Science*, 9, pp. 508-512.

Palácio, S., Espinoza-Quiñones, F., Módenes, A., Manenti, D., Oliveira, C. and Garcia, J. (2012). Optimised photocatalytic degradation of a mixture of azo dyes using a TiO_2 /H_2O_2 /UV process. *Water Science & Technology*, 65, pp. 1392-1398.

Pamt, H., Park, C., Kim, H. and Kim, C. (2013). Reduced graphene sheets decorated with ZnO flowers by hydrothermal process. *TMS2013 Supplemental Proceedings*, pp. 1-10.

Pang, Y. and Abdullah, A. (2013). Current status of textile industry wastewater management and research progress in malaysia: A review. *Clean Soil Air Water*, 41, pp. 751-764.

Panizza, M., Barbucci, A., Ricotti, R. and Cerisola, G. (2007). Electrochemical degradation of methylene blue. *Separation and Purification Technology*, 54, pp. 382-387.

Papić, S., Peternel, I., Krevzelj, Ž., Kušić, H. and Koprivanac, N. (2014). Advanced oxidation of an azo dye and its synthesis intermediates in aqueous solution: effect of fenton treatment on mineralization, biodegradability and toxicity. *Environmental Engineering & Management Journal*, 13, pp. 2561-2571.

Park, S., Song, H., Lee, C., Hwang, S. and Cho, I. (2015). Enhanced photocatalytic activity of ultrathin $Ba_5Nb_4O_{15}$ two-dimensional nanosheets. *ACS Applied Materials and Interfaces*, 7, pp. 21860-21867.

Patil, S., Bethi, B., Sonawane, G., Shrivastava, V. and Sonawane, S. (2016). Efficient adsorption and photocatalytic degradation of Rhodamine B dye over Bi_2O_3-bentonite nanocomposites: A kinetic study. *Journal of Industrial and Engineering Chemistry*, 34, pp. 356-363.

Paul, R. (2015). *Denim: Manufacture, Finishing and Applications*. 1st ed. [ebook] Elsevier, p. 550. Available at: https://books.google.com.my/books?isbn=0857098497 [Accessed 22 Mar. 2016].

Perry, D. (2016). *Handbook of Inorganic Compounds*. 2nd ed. [ebook] CRC Press, p. 68. Available at: https://books.google.com.my/books?isbn=1439814627 [Accessed 28 Jul. 2016].

Petrović, M., Mitrović, J., Antonijević, M., Matović, B., Bojić, D. and Bojić, A. (2015). Synthesis and characterization of new Ti–Bi_2O_3 anode and its use for reactive dye degradation. *Materials Chemistry and Physics*, 158, pp. 31-37.

Poulios, I., Micropoulou, E., Panou, R. and Kostopoulou, E. (2003). Photooxidation of eosin Y in the presence of semiconducting oxides. *Applied Catalysis B: Environmental*, 41, pp. 345-355.

Poyatos, J., Muñio, M., Almecija, M., Torres, J., Hontoria, E. and Osorio, F. (2009). Advanced oxidation processes for wastewater treatment: state of the art. *Water Air Soil Pollution*, 205, pp. 187-204.

Pradhan, G. and Parida, K. (2010). Fabrication of iron-cerium mixed oxide: an efficient photocatalyst for dye degradation. *International Journal of Engineering, Science and Technology*, 2, pp. 53-65.

Puentes-Cárdenas, I., Chávez-Camarillo, G., Flores-Ortiz, C., Cristiani-Urbina, M., Netzahuatl-Muñoz, A., Salcedo-Reyes, J., Pedroza-Rodríguez, A. and Cristiani-Urbina, E. (2016). Adsorptive removal of acid blue 80 dye from aqueous solutions by Cu-TiO_2. *Journal of Nanomaterials*, 2016, pp. 1-15.

Qiu, S., Xu, S., Li, G. and Yang, J. (2016). Synergetic effect of ultrasound, the heterogeneous fenton reaction and photocatalysis by TiO_2 loaded on nickel foam on the degradation of pollutants. *Materials*, 9, pp. 1-13.

Rahmani, A., Godini, K., Nematollahi, D., Azarian, G. and Maleki, S. (2015). Degradation of azo dye C.I. Acid Red 18 using an eco-friendly and continuous

electrochemical process. *Korean Journal of Chemical Engineering*, 33, pp. 532-538.

Rai, M., Bhat, P., Prajna, P., Jayadev, K. and Rao, P. (2014). Degradation of malachite green and congo red using *Aloe barabadensis* Mill. Extract. *International Journal of Current Microbiology and Applied Sciences*, 3, pp. 330–340.

Rajabi, H. and Farsi, M. (2015). Effect of transition metal ion doping on the photocatalytic activity of ZnS quantum dots: synthesis, characterization, and application for dye decolorization. *Journal of Molecular Catalysis A: Chemical*, 399, pp. 53-61.

Rajabi, H., Khani, O., Shamsipur, M. and Vatanpour, V. (2013). High-performance pure and Fe^{3+}-ion doped ZnS quantum dots as green nanophotocatalysts for the removal of malachite green under UV-light irradiation. *Journal of Hazardous Materials*, 250, pp. 370–378.

Rauf, M. and Ashraf, S. (2009). Fundamental principles and application of heterogeneous photocatalytic degradation of dyes in solution. *Chemical Engineering Journal*, 151, pp. 10-18.

Rauf, M., Meetani, M. and Hisaindee, S. (2011). An overview on the photocatalytic degradation of azo dyes in the presence of TiO_2 doped with selective transition metals. *Desalination*, 276, pp. 13-27.

Raza, W., Haque, M., Muneer, M., Harada, T. and Matsumura, M. (2015). Synthesis, characterization and photocatalytic performance of visible light induced bismuth oxide nanoparticle. *Journal of Alloys and Compounds*, 648, pp. 641-650.

Raza, W., Khan, A., Alam, U., Muneer, M. and Bahnemann, D. (2016). Facile fabrication of visible light induced Bi_2O_3 nanorod using conventional heat treatment method. *Journal of Molecular Structure*, 1107, pp. 39-46.

Ruslimie, C., Razali, H. and Khairul, W. (2011). Catalytic study on TiO_2 photocatalyst synthesised via microemulsion method on atrazine. *Sains Malaysiana*, 40, pp. 897-902.

Saggioro, E., Oliveira, A., Pavesi, T., Maia, C., Ferreira, L. and Moreira, J. (2011). Use of titanium dioxide photocatalysis on the remediation of model textile wastewaters containing azo dyes. *Molecules*, 16, pp.10370-10386.

Saikia, L., Bhuyan, D., Saikia, M., Malakar, B., Dutta, D. and Sengupta, P. (2015). Photocatalytic performance of ZnO nanomaterials for self-sensitized degradation of malachite green dye under solar light. *Applied Catalysis A: General*, 490, pp. 42-49.

Salazar-Pérez, A., Camacho-López, M., Morales-Luckie, R., Sánchez-Mendieta, V., Ureña-Núñez, F. and Arenas-Alatorre, J. (2005). Structural evolution of Bi_2O_3 prepared by thermal oxidation of bismuth nano-particles. *Superficies y vacío*, 18, pp. 4-8.

Salleh, M., Mahmoud, D., Karim, W. and Idris, A. (2011). Cationic and anionic dye adsorption by agricultural solid wastes: A comprehensive review. *Desalination*, 280, pp. 1-13.

Samarghandi, M., Rahmani, A., Samadi, M., Kiamanesh, M. and Azarian, G. (2015). Degradation of pentachlorophenol in aqueous solution by the UV/ZrO_2/H_2O_2 photocatalytic process. *Avicenna Journal of Environmental Health Engineering*, (In Press).

Sanatgar-Delshade, E., Habibi-Yangjeh, A. and Khodadadi-Moghaddam, M. (2011). Hydrothermal low-temperature preparation and characterization of ZnO nanoparticles supported on natural zeolite as a highly efficient photocatalyst. *Monatshefte für Chemie - Chemical Monthly*, 142, pp. 119-129.

Sapawe, N., Jalil, A. and Triwahyono, S. (2013). Photodecolorization of methylene blue over EGZrO_2/EGZnO/EGFe_2O_3/HY photocatalyst: effect of radical scavenger. *Malaysian Journal of Fundamental and Applied Sciences*, 9, pp. 67-73.

Saratale, R., Saratale, G., Chang, J. and Govindwar, S. (2010). Decolorization and biodegradation of reactive dyes and dye wastewater by a developed bacterial consortium. *Biodegradation*, 21, pp. 999-1015.

Saratale, R., Saratale, G., Chang, J. and Govindwar, S. (2011). Bacterial decolorization and degradation of azo dyes: A review. *Journal of the Taiwan Institute of Chemical Engineers*, 42, pp. 138-157.

Saratale, R., Saratale, G., Kalyani, D., Chang, J. and Govindwar, S. (2009). Enhanced decolorization and biodegradation of textile azo dye Scarlet R by using developed microbial consortium-GR. *Bioresource Technology*, 100, pp. 2493-2500.

Sasikala, R., Karthikeyan, K., Easwaramoorthy, D., Bilal, I. and Rani, S. (2016). Photocatalytic degradation of trypan blue and methyl orange azo dyes by cerium loaded CuO nanoparticles. *Environmental Nanotechnology, Monitoring & Management*, 6, pp. 45-53.

Schlesinger, M., Weber, M., Schulze, S., Hietschold, M. and Mehring, M. (2013). Metastable β-Bi_2O_3 nanoparticles with potential for photocatalytic water purification using visible light irradiation. *ChemistryOpen*, 2, pp. 146-155.

Scialdone, O., D'Angelo, A. and Galia, A. (2015). Energy generation and abatement of Acid Orange 7 in reverse electrodialysis cells using salinity gradients. *Journal of Electroanalytical Chemistry*, 738, pp. 61-68.

Shanthi, M. and Kuzhalosai, V. (2012). Photocatalytic degradation of an azo dye, acid red 27, in aqueous solution using nano ZnO. *Indian Journal of Chemistry*, 51A, pp. 428-434.

Sharma, D., Bansal, A., Ameta, R. and Sharma, H. (2011). Use of semiconducting bismuth oxide in photocatalytic bleaching of Malachite green. *Asian J. Research Chem.*, 4, pp. 1393-1296.

Sharma, D., Bansal, A., Ameta, R. and Sharma, H. (2013). Photodegradation of Azure B with the help of bismuth oxide and bismuth sulphide used as photocatalytic: A comparative study. *International Journal of Chemtech Research*, 5, pp. 578-584.

Singh, R., Singh, P. and Singh, R. (2015). Enzymatic decolorization and degradation of azo dyes – A review. *International Biodeterioration & Biodegradation*, 104, pp. 21-31.

Solís, M., Solís, A., Pérez, H., Manjarrez, N. and Flores, M. (2012). Microbial decolouration of azo dyes: A review. *Process Biochemistry*, 47, pp. 1723-1748.

Sood, S., Umar, A., Kumar Mehta, S. and Kumar Kansal, S. (2015). α-Bi_2O_3 nanorods: An efficient sunlight active photocatalyst for degradation of Rhodamine B and 2,4,6-trichlorophenol. *Ceramics International*, 41, pp. 3355-3364.

Soroodan Miandoab, E. and Fatemi, S. (2015). Upgrading TiO_2 photoactivity under visible light by synthesis of MWCNT/TiO_2 nanocomposite. *International Journal of Nanoscience and Nanotechnology*, 11, pp. 1-12.

Sreelatha, S., Velvizhi, G., Reddy, C., Modestra, J. and Mohan, S. (2015). Solid electron acceptor effect on biocatalyst activity in treating azo dye based wastewater. *RSC Adv.*, 5, pp. 95926-95938.

Sreethawong, T. (2012). Mesoporous-assembled nanocrystal photocatalysts for degradation of azo dyes. In: S. Sharma and R. Sanghi, ed., *Advances in Water Treatment and Pollution Prevention*, 1st ed. [online] Springer Netherlands, pp. 147-175. Available at: https://books.google.com.my/books?isbn=9400742045 [Accessed 22 Mar. 2016].

Su, H., Cao, S., Xia, N., Huang, X., Yan, J., Liang, Q. and Yuan, D. (2014). Controllable growth of Bi_2O_3 with rod-like structures via the surfactants and its electrochemical properties. *J Appl Electrochem*, 44, pp. 735-740.

Sullivan, J., Neville, E., Herron, R., Thampi, K. and MacElroy, J. (2014). Routes to visible light active C-doped TiO_2 photocatalysts using carbon atoms from the Ti precursors. *Journal of Photochemistry and Photobiology A: Chemistry*, 289, pp. 60-65.

Sun, Y., Wang, W., Zhang, L. and Zhang, Z. (2012). Design and controllable synthesis of α-/γ-Bi_2O_3 homojunction with synergetic effect on photocatalytic activity. *Chemical Engineering Journal*, 211-212, pp. 161-167.

Suwanboon, S., Amornpitoksuk, P. and Muensit, N. (2011). Dependence of photocatalytic activity on structural and optical properties of nanocrystalline ZnO powders. *Ceramics International*, 37, pp. 2247-2253.

Tan, L., He, M., Song, L., Fu, X. and Shi, S. (2016). Aerobic decolorization, degradation and detoxification of azo dyes by a newly isolated salt-tolerant yeast Scheffersomyces spartinae TLHS-SF1. *Bioresource Technology*, 203, pp. 287-294.

Tan, L., Li, H., Ning, S. and Xu, B. (2014). Aerobic decolorization and degradation of azo dyes by suspended growing cells and immobilized cells of a newly isolated yeast Magnusiomyces ingens LH-F1. *Bioresource Technology*, 158, pp. 321-328.

Tan, L., Ning, S., Zhang, X. and Shi, S. (2013). Aerobic decolorization and degradation of azo dyes by growing cells of a newly isolated yeast Candida tropicalis TL-F1. *Bioresource Technology*, 138, pp. 307-313.

Tayeb, A. and Hussein, D. (2015). Synthesis of TiO_2 nanoparticles and their photocatalytic activity for Methylene Blue. *American Journal of Nanomaterials*, 3, pp. 57-63.

Tchobanoglous, G., Burton, F. and Stensel, H. (2003). *Wastewater engineering*. Boston: McGraw-Hill, pp. 1131.

Thompson, M. (2010). *Synthesis and characterization of δ-Bi_2O_3 related materials sstabilized by Substitutions of Ca, Ga, Nb and Re.* Ph.D. University of Birmingham.

Tseng, D., Juang, L. and Huang, H. (2012). Effect of oxygen and hydrogen peroxide on the photocatalytic degradation of monochlorobenzene in aqueous suspension. *International Journal of Photoenergy*, 2012, pp. 1-9.

Venkatachalam, N., Palanichamy, M., Arabindoo, B. and Murugesan, V. (2007). Enhanced photocatalytic degradation of 4-chlorophenol by Zr^{4+} doped nano TiO_2. *Journal of Molecular Catalysis A: Chemical*, 266, pp. 158-165.

Verma, A., Dash, R. and Bhunia, P. (2012). A review on chemical coagulation/flocculation technologies for removal of colour from textile wastewaters. *Journal of Environmental Management*, 93, pp. 154-168.

Vignesh, K., Rajarajan, M. and Suganthi, A. (2014). Visible light assisted photocatalytic performance of Ni and Th co-doped ZnO nanoparticles for the degradation of methylene blue dye. *Journal of Industrial and Engineering Chemistry*, 20, pp. 3826-3833.

Vijayaraghavan, J., Basha, S. and Jegan, J. (2013). A review on efficacious methods to decolorize reactive azo dye. *Journal of Urban and Environmental Engineering*, 7, pp. 30-47.

Viswanathan, V., Hansen, H. and Nørskov, J. (2015). Selective electrochemical generation of hydrogen peroxide from water oxidation. *Journal of Physical Chemistry Letters*, 6, pp. 4224-4228.

Wang, C., Shao, C., Wang, L., Zhang, L., Li, X. and Liu, Y. (2009). Electrospinning preparation, characterization and photocatalytic properties of Bi_2O_3 nanofibers. *Journal of Colloid and Interface Science*, 333, pp. 242-248.

Wang, H. and Rogach, A. (2014). Hierarchical SnO_2 nanostructures: Recent advances in design, synthesis, and applications. *Chemistry of Materials*, 26, pp. 123-133.

Wang, S., Zhu, Z., Coomes, A., Haghseresht, F. and Lu, G. (2005). The physical and surface chemical characteristics of activated carbons and the adsorption of methylene blue from wastewater. *Journal of Colloid and Interface Science*, 284, pp. 440-446.

Wang, Y., Zhao, J. and Wang, Z. (2011). A simple low-temperature fabrication of oblique prism-like bismuth oxide via a one-step aqueous process. *Colloids and Surfaces A: Physicochemical and Engineering Aspects*, 377, pp. 409-413.

Waring, D. and Hallas, G. (2013). *The chemistry and application of dyes*. 1st ed. [ebook] Springer Science & Business Media, p.31. Available at: https://books.google.com.my/books?isbn=1468477153 [Accessed 28 Feb. 2016].

Wu, S. and Chen, D. (2004). Synthesis of high-concentration Cu nanoparticles in aqueous CTAB solutions. *Journal of Colloid and Interface Science*, 273, pp. 165-169.

Wu, Y., Chaing, Y., Huang, C., Wang, S. and Yang, H. (2013). Morphology-controllable Bi_2O_3 crystals through an aqueous precipitation method and their photocatalytic performance. *Dyes and Pigments*, 98, pp. 25-30.

Xia, Y., Xiong, Y., Lim, B. and Skrabalak, S. (2009). Shape-controlled synthesis of metal nanocrystals: simple chemistry meets complex physics? *Angewandte Chemie International Edition*, 48, pp. 60-103.

Xiao, X., Hu, R., Liu, C., Xing, C., Qian, C., Zuo, X., Nan, J. and Wang, L. (2013). Facile large-scale synthesis of β-Bi_2O_3 nanospheres as a highly efficient photocatalyst for the degradation of acetaminophen under visible light irradiation. *Applied Catalysis B: Environmental*, 140-141, pp. 433-443.

Xu, H., Wu, L., Zhao, H., Jin, L. and Qi, S. (2015). Synergic effect between adsorption and photocatalysis of metal-free g-C_3N_4 derived from different precursors. *Public Library of Science One*, 10, pp. 1-20.

Yagub, M., Sen, T., Afroze, S. and Ang, H. (2014). Dye and its removal from aqueous solution by adsorption: A review. *Advances in Colloid and Interface Science*, 209, pp. 172-184.

Yang, Q., Li, C., Li, H., Li, Y. and Yu, N. (2009). Degradation of synthetic reactive azo dyes and treatment of textile wastewater by a fungi consortium reactor. *Biochemical Engineering Journal*, 43, pp. 225-230.

Yin, L., Niu, J., Shen, Z. and Chen, J. (2010). Mechanism of reductive decomposition of pentachlorophenol by Ti-Doped β-Bi_2O_3 under visible light irradiation. *Environmental Science & Technology*, 44, pp. 5581-5586.

You, S. and Teng, J. (2009). Anaerobic decolorization bacteria for the treatment of azo dye in a sequential anaerobic and aerobic membrane bioreactor. *Journal of the Taiwan Institute of Chemical Engineers*, 40, pp. 500-504.

Yuan, T. and Sun, R. (2010). Modification of straw for activated carbon preparation and application for the removal of dyes from aqueous solutions. *Cereal Straw as a Resource for Sustainable Biomaterials and Biofuels*, pp. 239-252.

Zhang, D., Chen, L., Xiao, C., Feng, J., Liao, L., Wang, Z. and Wei, T. (2016). Facile synthesis of high {001} facets dominated BiOCl nanosheets and their selective dye-sensitized photocatalytic activity induced by visible light. *Journal of Nanomaterials*, 2016, pp. 1-7.

Zhang, L., Wang, W., Yang, J., Chen, Z., Zhang, W., Zhou, L. and Liu, S. (2006). Sonochemical synthesis of nanocrystallite Bi_2O_3 as a visible-light-driven photocatalyst. *Applied Catalysis A: General*, 308, pp. 105-110.

Zhang, W., Shen, R., Lu, K., Ji, A. and Cao, Z. (2012). Nanoparticle enhanced evaporation of liquids: A case study of silicone oil and water. *AIP Advances*, 2, pp. 042119

Zhang, X., Liu, X., Fan, C., Wang, Y., Wang, Y. and Liang, Z. (2013). A novel BiOCl thin film prepared by electrochemical method and its application in photocatalysis. *Applied Catalysis B: Environmental*, 132-133, pp. 332-341.

Zhao, C., Yang, Y. and Zhang, Z. (2012). Photocatalytic treatment of microcystin-lr-containing wastewater using Pt/WO_3 nanoparticles under simulated solar light. *Open Journal of Applied Sciences*, 2, pp. 86-92.

Zhou, X. and Xiang, X. (2013). Effect of different plants on azo-dye wastewater bio-decolorization. *Procedia Environmental Sciences*, 18, pp. 540-546.

Zhu, L., Wei, B., Xu, L., Lü, Z., Zhang, H., Gao, H. and Che, J. (2012). $Ag_2O–Bi_2O_3$ composites: synthesis, characterization and high efficient photocatalytic activities. *CrystEngComm*, 14, pp. 5705-5709.

APPENDICES

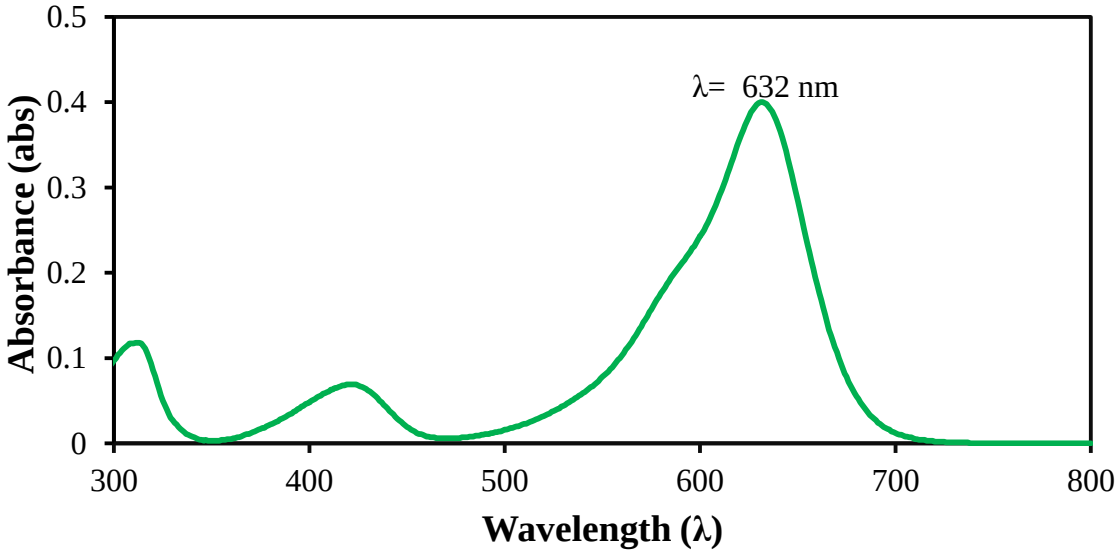

Appendix 1: MG wavelength scan

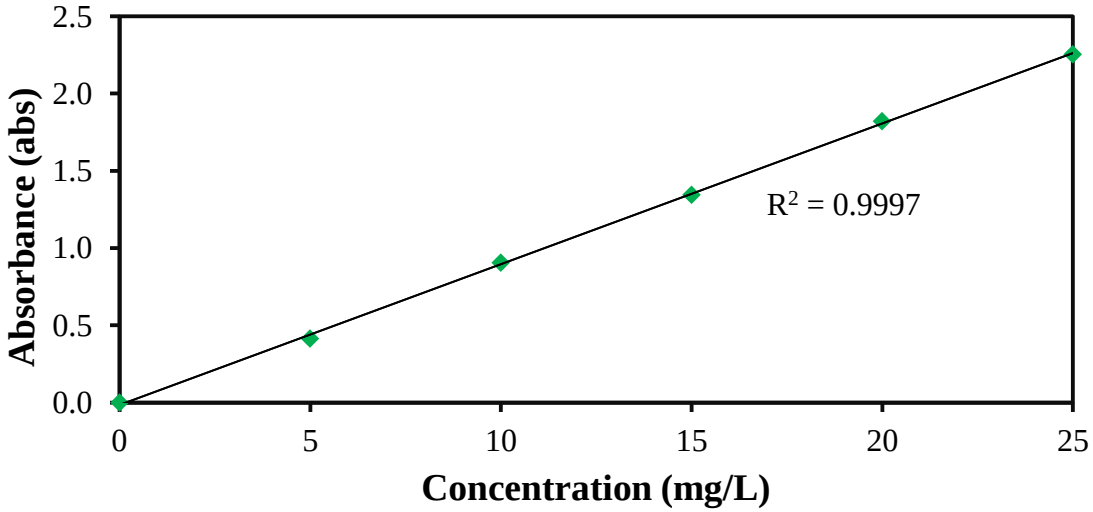

Appendix 2: MG calibration curve

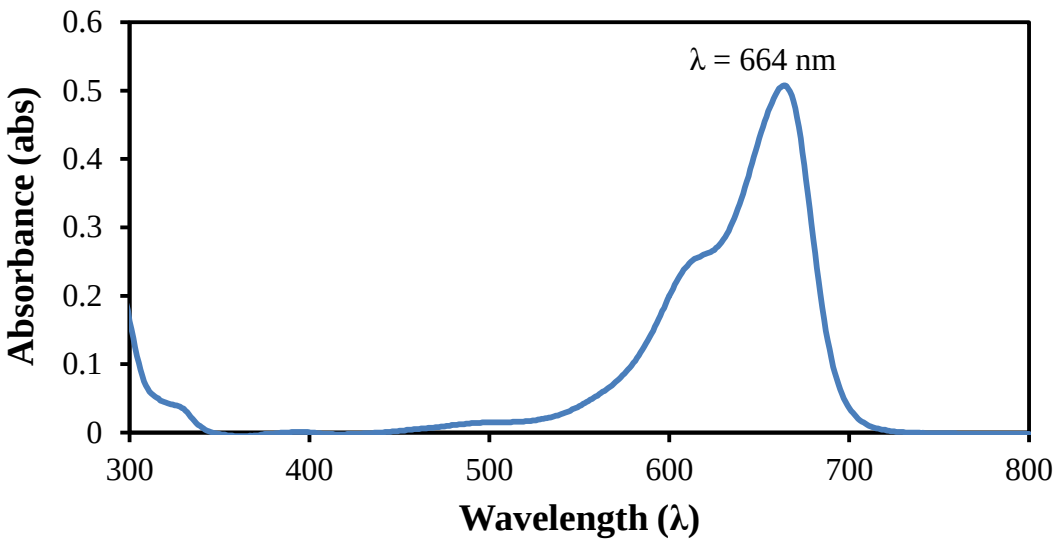

Appendix 3: MB wavelength scan

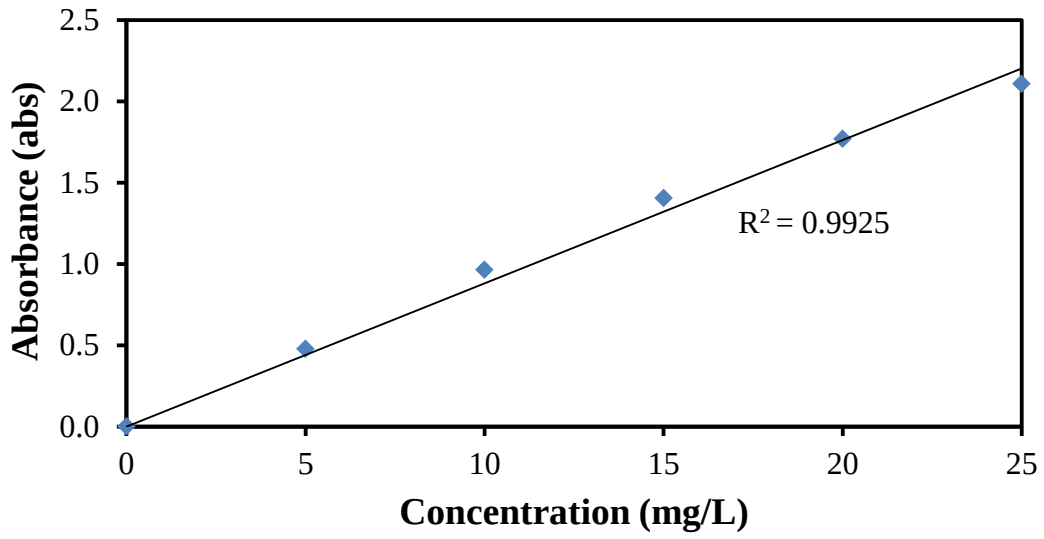

Appendix 4: MB calibration curve

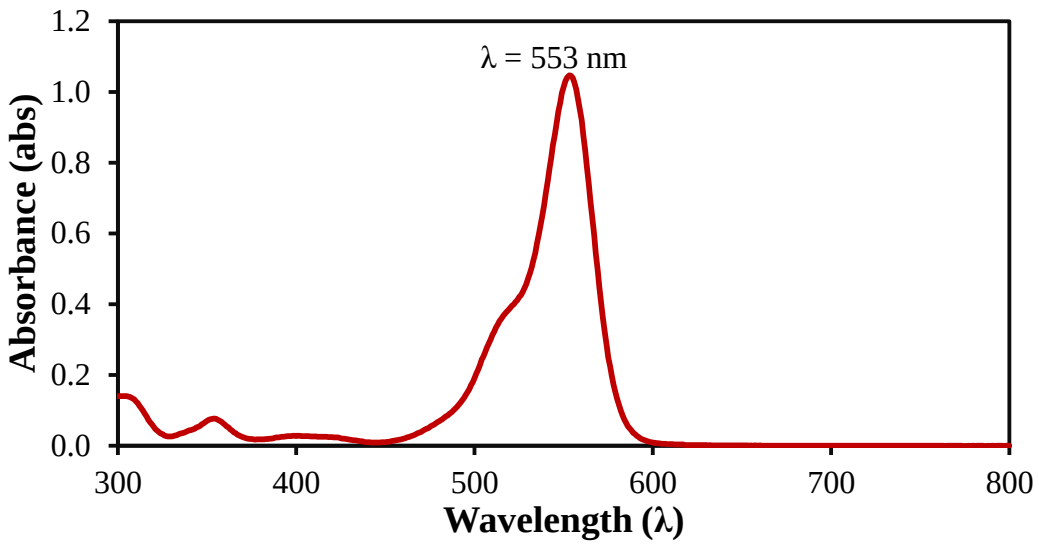

Appendix 5: RhB wavelength scan

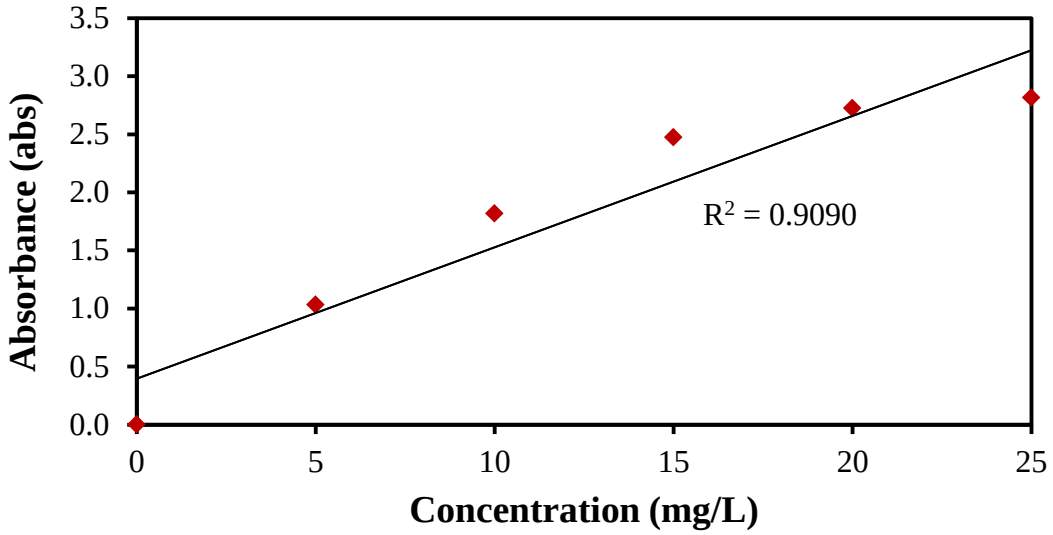

Appendix 6: RhB calibration curve

PUBLICATION

Lam, S.M., Sin, J.C. and Christina Previtha A/P J.D. (2016). Facile synthesis of Bi_2O_3 nanoflakes and their visible light-driven catalytic activity. *Material Letters* (submitted).